

# Geologic Map of the Nevada Part of the Desert Quadrangle and Adjacent Part of the McCullough Mountain Quadrangle, Clark County, Nevada

by

Michael H. Darin<sup>1</sup>, Andrew V. Zuza<sup>1</sup>, Seth Dee<sup>1</sup>, and Racheal L. Johnsen<sup>2</sup>

<sup>1</sup>Nevada Bureau of Mines and Geology, University of Nevada, Reno

<sup>2</sup>Department of Geoscience, University of Nevada, Las Vegas

2022

*Disclaimer: NBMG open-file reports have not undergone formal peer review. This geologic map was funded by the U.S. Geological Survey Earth Mapping Resources Initiative (MRI), Cooperative Agreement G19AC00255.*

## DESCRIPTION OF MAP UNITS

### Quaternary Deposits

Eolian deposits shown on the Desert quadrangle were compiled directly from mapping by House et al. (2006).

**Qe** **Eolian sand (Holocene to late Pleistocene)** Deposits of windblown sand and minor silt. Planar to undulatory sheets of sand deposited on inactive alluvial surfaces. Exposed thickness of the unit is typically 1–3 m.

**Qea** **Mixed eolian sand and alluvium (Holocene to late Pleistocene)** Thin (<1m) deposits of windblown sand and minor silt that overlie inactive alluvial-fan surfaces, likely Qfi. Eolian sand is locally intermingled with or overlain by a lag of loose gravel resulting from the eolian inflation of desert pavement surfaces.

**Qc** **Colluvium (Holocene to late Pleistocene)** Angular to slightly rounded, poorly sorted boulders to pebbles in a variably sandy matrix. Present at the base of steep bedrock slopes. Colluvium deposits generally grade into, and are commonly included within, alluvial fan map units. Where colluvium is distinguished it is undivided by age and includes very young unconsolidated deposits through semi-consolidated abandoned surfaces. Soil development varies from minimal to stage II CaCO<sub>3</sub> Bk horizons. Exposed thickness of the unit is less than 5 m.

Alluvial-fan deposits are divided on the basis of surficial, morphologic, and pedogenic characteristics outlined by House et al. (2006, 2010) for their mapping in the Ivanpah Valley. Mapping from the House et al. (2006) geologic map publication partially overlaps with the Desert quadrangle and formed the basis for some of the linework presented in

this publication; however, the unit names differ with correlative unit names presented in the unit descriptions below.

**Qfy** **Young alluvial-fan deposits (Holocene)** Coarse-grained alluvial deposits in intermittently active to recently abandoned alluvial fans and washes; typically sandy pebble-to cobble-sized gravel with boulders. At range fronts, Qfy grades into and includes young pediment veneers of colluvium. Clasts are subrounded to subangular. Surfaces have complex distributary flow patterns with morphology ranging from fresh bar-and-channel forms to slightly smoothed surfaces with moderately developed gravel pavement and light rock varnish. Includes youngest abandoned surfaces and terraces 0.25–2 m above active washes. Typically has weak to no soil development. If present, soil development is characterized by Stage I, CaCO<sub>3</sub> coatings on bottoms of clasts. Miller et al. (2010) present radiocarbon and luminescence dates ranging from 3–6 ka collected from Mojave Desert alluvial-fan deposits (their unit Qya<sub>3</sub>) correlative with the recently abandoned Qfy alluvial-fan surfaces in this study. The Qfy map unit is correlative with units Qay<sub>3</sub> and Qay<sub>2</sub> in House et al. (2006). Exposed thickness of the unit is typically 1–4 m.

**Qfi** **Intermediate-aged alluvial-fan deposits (early Holocene to late Pleistocene)** Coarse-grained alluvial deposits in inactive alluvial fans and terraces. Grain size at range fronts comprised largely of boulder-gravels, grading basinward to pebble-cobble gravels. At range fronts Qfi includes abandoned, moderately cemented pediment veneers of colluvium. Clasts are commonly subangular to subrounded. Coarse deposits are typically clast supported with a basinward increase in matrix support; weakly stratified throughout. Soils are characterized by Stage I+ to

II+ CaCO<sub>3</sub> Bk horizons, with carbonate clast coatings that vary from thin layers on the bottom of clasts to complete clast coatings up to 3 mm thick. In most locations, surface morphology is distinctively planar with a moderately to strongly developed desert pavement. Very coarse, boulder-rich deposits adjacent to range fronts have a muted bar-and-swale depositional morphology preserved. Surface clasts have moderate to dark rock varnish, which commonly gives the fans a distinctive dark color in aerial imagery. In most locations Qfi is comprised of 2–3 different-aged surfaces that were not divided. Qfi is locally buried by Qfy deposits but commonly elevated 2–6 m above incised Qfy channels and fans. Correlative alluvial-fan deposits in the Mojave Desert dated by Miller et al. (2010; their unit Qya<sub>4</sub>) and McDonald et al. (2003; their units Qf<sub>4</sub> and Qf<sub>5</sub>) yielded ages ranging from 9–29 ka. The Qfi map unit is correlative with unit Qay<sub>1</sub> in House et al. (2006). Exposed thickness of the unit rarely exceeds 5 m.

**Qfo Older alluvial-fan deposits (middle to early Pleistocene)** Coarse grained alluvial deposits in inactive or relict alluvial-fans and terraces. Grain size at range fronts comprised largely of boulder-gravels, grading basinward to pebble-cobble gravels. Clasts are commonly subangular to subrounded. Soils are characterized by Stage III to IV CaCO<sub>3</sub> Bk horizons, with pedogenic carbonate forming a continuous 0.75–2.5 m thick layer with local development of laminar carbonate structure. Upper soil horizons locally stripped. Surfaces are highly dissected by 1–5 m deep channels with a tributary pattern. Surface morphology varies from planar and smooth with erosionally rounded margins to fully rounded erosional remnants. Planar surfaces have tightly packed gravel pavement, very dark varnish, and some surface litter of pedogenic carbonate clasts. Pedogenic carbonate litter gives Qfo fans a distinctive lighter colored appearance relative to Qfi in aerial imagery. Surface clasts have dark rock varnish. Topographic separation from Qfi fans varies from minimal to over 5 m. In most locations, Qfo is comprised of 2–3 different-aged surfaces that were not divided. Luminescence ages from the northeastern Mojave Desert date a correlative alluvial-fan unit at 33–140 ka (unit Qia in Mahan et al., 2007). The Qfo map unit is correlative with units Qai and Qao in House et al. (2006). Exposed thickness of the unit ranges from 5 to ~10 m.

**QTls Old landslide deposits (early Pleistocene to Pliocene?)** Deposits of jumbled boulders at one location along the western range front of the Lucy Gray Mountains. Sub-rounded boulders of orthogneiss with long axes up to 5 m mantle the surface of the deposit. Overlies map unit QTf and is displaced by faults along the western Lucy Gray Mountains range front. Exposed thickness of the unit is 15–20 m.

**QTf Oldest alluvial-fan deposits (early Pleistocene to Pliocene?)** Coarse-grained alluvial deposits in relict alluvial fans and high-standing alluvial deposits abandoned by deep dissection. Grain size comprised largely of boulder-gravels with subangular to subrounded clasts. Soils are locally stripped, where preserved QTf soils are characterized

by Stage IV to VI CaCO<sub>3</sub> Bk horizons, with pedogenic carbonate forming a continuous 2–4+ m thick layer with common laminar carbonate structure and local brecciation. Morphology varies from deeply dissected topography with roughly concordant ridge crests to fully eroded, isolated ballenas with discordant ridge crests. At range fronts high-standing erosional remnants of QTf deposits commonly overlie exposed bedrock erosion surfaces. Desert pavement is rarely preserved. The deposit surface is commonly characterized by a rubble layer of broken fragments of petrocalcic fragments giving the unit a very light color in aerial imagery. Topographic crests of the QTf deposits are commonly 5–15+ m above active washes. QTf deposits are not characterized by broadly concordant surface and likely span a broad age range from the early Pleistocene to the Pliocene. Displaced by faults along the western Lucy Gray Mountains range front. The QTf map unit is correlative with unit QTa in House et al. (2006). Exposed thickness of the unit ranges from 5 to 50 m.

## Tertiary Igneous and Sedimentary Rocks

**Tbs Tuff of Bridge Spring (middle Miocene)** Light gray to purple, subwelded to densely welded, crystal-lithic rhyolite ash-flow tuff (fig. 1; table 1) with up to 15% subhedral phenocrysts (0.5–3 mm) of quartz > sanidine > biotite + sphene + accessory plagioclase. This unit is a regionally extensive ignimbrite marker bed that occurs throughout Eldorado Valley and the McCullough Range (e.g., Faulds et al., 2002, Smith et al., 2010). Within the map area, the base commonly displays a 1–1.5 m thick basal vitrophyre that contains abundant (up to 35%) large (2–5 mm) subhedral to euhedral quartz and sanidine phenocrysts and conspicuous angular xenoliths of Proterozoic and Tertiary volcanic porphyry. Grayish purple to maroon fiamme up to 13 cm long occur within the first 3–4 m above the vitrophyre. Dark gray to black or maroon, angular aphanitic to porphyritic basaltic andesite lithic fragments are common and locally abundant (10–15%), as are small (<1 cm) angular white pumice with quartz, sanidine, and biotite. Tbs is discontinuously exposed along the eastern edge of the map area, where it forms relatively resistant ridges that weather gray to tan. We report an <sup>40</sup>Ar/<sup>39</sup>Ar age of 15.21 ± 0.10 Ma for this unit (sample 11-LG58; fig. 2, tables 2 and 3). Thickness varies from 0–30 m.

**Tcs Conglomerate and sandstone (middle to early Miocene)** Tan conglomerate and medium-grained sandstone and pebbly sandstone. Conglomerate is typically massive to crudely bedded, unsorted, well cemented sandy pebble-cobble conglomerate with mixed matrix and clast support and a fine- to medium-grained sand matrix. Clasts are dominantly subangular to angular volcanic rocks that predominantly consist of dark gray vesicular and scoriaceous clinopyroxene-plagioclase-olivine basaltic andesite (Tba) and light gray hornblende dacite (Tdh). Sandstones are typically fine- to coarse-grained, subangular, moderately well sorted, arkosic, and dominated by volcanic lithic fragments. Normal grading and trough cross-bedding

are uncommon. Clasts of Precambrian crystalline basement units are very rare; their notable absence helps to distinguish this unit from the Tertiary basal conglomerate (Tcb) and from Quaternary alluvial-fan deposits, all of which are dominated by Precambrian lithologies. Interpreted as debris flow deposits in an alluvial-fan setting, probably associated with regional extension beginning at ca. 16–15 Ma. East-dipping deposits of Tcs are exposed in the basin between the Lucy Gray Mountains and the McCullough Range, and equivalent sediments are presumed to underlie Ivanpah Valley. Thickness is uncertain, but gravity data suggests basin sediments on either side of the southern Lucy Gray Mountains range from <300 to 600 m thick (Miller et al., 2019; Denton and Ponce, 2018; Denton et al., 2020).

**Tap Porphyritic andesite (middle to early Miocene)** Porphyritic, medium gray trachyandesite (fig. 1) lavas and minor autobreccia. Contains 10–15% euhedral and relatively fresh phenocrysts of clinopyroxene >> plagioclase > biotite = hornblende in a gray, fine-grained groundmass. Tap distinctly lacks olivine and vesicles, both of which distinguish it from Tba. Weathers rusty brown to black with an uncommon vuggy texture and/or significant desert varnish locally. Tap is only exposed in the eastern part of the map area, where it has a thickness of at ~30–40 m.

**Tba Basaltic andesite (middle to early Miocene)** Resistant, ridge-forming unit consisting of dark gray, vesicular, porphyritic basaltic trachyandesite to trachyandesite lava flows (fig. 1) containing abundant (10–15%) large clinopyroxene and plagioclase phenocrysts up to 7 mm long, and subordinate sub-mm olivine altered to iddingsite, set in a dense gray groundmass. Locally displays red unsorted, clast-supported autobreccias. In the northern Lucy Gray Mountains, Tba contains thin, unmapped interbeds of tan, well-cemented (with calcite), arkosic to grussy granular sandstone composed of mostly quartz > potassium feldspar > plagioclase, and <2% volcanic lithic fragments of clinopyroxene-phyric basalt. Although undated, stratigraphic relations indicate an age between ca. 18 and 15.2 Ma for this unit and correlation with the Patsy Mine Volcanics (Anderson, 1971; Smith et al., 2010) and the volcanic rocks of Dixie Mine and the Highland Range (Faulds et al., 2002). Thickness is uncertain though probably >50 m. Maximum thickness within the map area is ~300 m.

**Tdh Hornblende dacite (early Miocene)** Light gray, porphyritic dacite lava flows with up to 5% euhedral hornblende phenocrysts up to 5 mm long in a homogeneous, fine-grained, light gray groundmass composed of microlitic plagioclase. Locally displays a 2- to 4-cm-thick planar flow foliation defined by mm-scale crinkly lithophysae. Weathers medium gray to pale orange and breaks into slaty slabs and chips. Base of unit is locally a 1- to 5-m-thick breccia composed of angular pinkish-purple dacite clasts up to 20 cm wide. Although undated, Tdh is correlative with compositionally similar monolithologic breccias and block-and-ash flows (Tdht) dated at  $17.99 \pm 0.26$  Ma (table 2). Thickness is 40–70 m across the map area.

**Tdht Dacitic tuff breccias (early Miocene)** Slope-forming, massive, unsorted, monomict dacitic tuff breccias and block-and-ash flows correlative with compositionally similar lava flows of Tdh. Individual deposits range from gray to beige-pink or light purple. Most clasts are hornblende-phyric dacite (Tdh). A single tuff breccia deposit at base of unit contains a polymict volcanic clast assemblage that includes rare gneiss (Xog) clasts. We report a new zircon U-Pb age of  $17.99 \pm 0.26$  Ma from a block-and-ash flow near the base of this unit (sample 0309LG4, tables 2 and 4, fig. 3). Maximum thickness is ~120 m.

**Tps Peach Spring Tuff (early Miocene)** Light gray, unwelded to moderately welded crystal-lithic rhyolite ash-flow tuff (fig. 1) interbedded within basalt and basanite lava flows of Tbo. Contains abundant subhedral to euhedral quartz, sanidine, biotite, and minor plagioclase and hornblende. Northern exposures are pink to pale orange on fresh surfaces and weather to burnt orange. Tps commonly displays white pumice fiamme up to 7 cm long and rare small (<4 mm) subrounded gray to maroon aphanitic to microporphyritic volcanic lithic fragments, some of which are olivine- or clinopyroxene-phyric basalt or andesite (Tbo?). Southern exposures are laterally discontinuous, massive, friable, ashy, and distinctly nonwelded; these exposures also show scattered small (typically <7 mm) and equant white pumice and dark volcanic lithic fragments that make up <5% of the rock by volume. Laterally discontinuous deposits that become more pink and ashy with abundant white pumice near pinch-outs. We report an  $^{40}\text{Ar}/^{39}\text{Ar}$  age of  $18.62 \pm 0.16$  Ma for this tuff from a sample collected from the east-central part of the quadrangle (sample 11-LG27; fig. 2, tables 2 and 3). Thickness varies from 0–12 m in the map area.

**Tbo Olivine basalt (early Miocene)** Dark gray to black low-silica (~43 wt%  $\text{SiO}_2$ ) basalt to basanite lava flows and associated autobreccias (fig. 1). Lavas have a characteristically dense, nonvesicular, dark gray groundmass with 5–15% small olivine phenocrysts that are pervasively altered red to iddingsite, or less commonly serpentine. Except for uncommon flows that also contain up to 2% small (sub-mm) clinopyroxene, the absence of other phenocrysts is diagnostic of this unit. Intervening red oxidized autobreccias are up to 8 m thick and form prominent markers between lava flows. Weathered purplish gray to tan or rusty orange. Tbo usually rests directly on the nonconformity with Paleoproterozoic basement or on the basal conglomerate unit (Tcb). We report a new zircon U-Pb age of  $18.42 \pm 0.34$  Ma from an andesitic lava flow at the top of this unit (sample Fringe; fig. 3, tables 2 and 4), which is statistically similar to an  $^{40}\text{Ar}/^{39}\text{Ar}$  age of  $18.62 \pm 0.16$  Ma for the interbedded Peach Spring Tuff (table 2). Maximum thickness of Tbo is ~150 m.

**Tcb Basal conglomerate (early Miocene to late Oligocene)** Regionally recognized basal conglomerate unit composed of a diverse assemblage of igneous, metamorphic, and sedimentary clasts. Consists of poorly sorted and weakly cemented sandy pebble-cobble

conglomerate and pebbly sandstone, locally cross-bedded. Conglomerates show mixed matrix- and clast-support; matrix is composed of coarse-grained arkosic sand. Clasts are generally rounded to well-rounded and composed of orthogneiss, granite, diorite, garnet gneiss, gray Paleozoic limestone, quartzite, and reddish orange sandstone. Locally, the upper part (<10 m) of this unit is composed almost entirely of subangular, intermediate, porphyritic volcanic clasts with plagioclase>biotite. Tcb occurs as a discontinuous outcrop belt at the base of the Tertiary sequence, where it rests nonconformably on Precambrian crystalline units. It is correlative with the “McCullough Spring Conglomerate” of the northern Lucy Gray Mountains and southern McCullough Range (Herrington, 2000), the “Jean Conglomerate” (Hanson, 2008) and “Roundstone gravels” unit (Garside et al., 2012) farther north, and likely with the Rainbow Gardens formation and similar unnamed units in the Lake Mead region (Lamb et al., 2018, and references therein). An age of ~24–19 Ma has been assigned to the Jean conglomerate and Rainbow Gardens formation based on interbedded tuff and detrital zircon geochronology (Hanson, 2008; Lamb et al., 2018); a dacitic tuff interbed (sample MP21SD-1; fig. 1) within Tcb in the southernmost Lucy Gray Mountains was not dated in this study. Thickness in the map area varies from 0 to 60 m, but is typically less than 20 m.

## Paleoproterozoic Orthogneiss and Migmatite Gneiss

Naming conventions and unit assignments based on adjacent mapping of Dewitt et al. (1989) and Miller and Wooden (1993, 1994). Basement gneiss units are heterogeneously mixed, and map units were assigned based on most prominent lithology.

**Xbbp Beer Bottle Pass pluton** Very coarse grained, hornblende-biotite granite with euhedral to subhedral K-feldspar phenocrysts ~3–5 cm in length. Magmatic state to subsolidus fabrics developed across much of the pluton in the map area, but the pluton is less deformed to the north (Duebendorfer and Christensen, 1995). Subsolidus deformation shows top-east-southeast kinematics, similar to deformation observed in many of the Paleoproterozoic orthogneiss units. At one location in the northern part of the map area, Xeg is juxtaposed over Xbbp along a discrete mylonitic shear zone. This shear zone is best observed in the Xbbp unit with very fine-grained K-feldspar. Kinematics observed just outside of the mylonite show top-southeast shear sense, evidenced by S-C fabrics and asymmetric mantled porphyroclasts. The similar shear sense of this discrete shear zone and more distributed strain observed throughout the pluton in the study area are evidence that both reflect regional top-east deformation.

Almeida et al. (2016) provided a U-Pb age from a sample within the study area of  $1681.6 \pm 7.9$  Ma and  $1689.4 \pm 8.3$  Ma (table 2). We report two new U-Pb zircon ages of  $1663 \pm 6$  Ma from a sample (BBP1) just north of the map boundary, and  $1658 \pm 6$  Ma from a sample (BBP4) in the

central McCullough Range (fig. 3; tables 2 and 4). Within uncertainties, these ages confirm an age of ca. 1.66–1.68 Ga for the Beer Bottle Pass pluton. These constraints also suggest that the phase of deformation that impacted Xbbp was active during (?) and after ca. 1.68 Ga.

We also report a new zircon U-Pb age of  $1644 \pm 44$  Ma for the McClanahan Spring pluton in the central McCullough Range (sample 0204M1; fig. 3, tables 2 and 4), which suggests emplacement either coeval with or slightly younger than Xbbp.

**Xeg Equigranular granitic gneiss** Equigranular, generally light colored to leucocratic granite. Light color index due to sparseness of mafic phases makes its boundaries with Xbkg or Xbbp sharp in aerial imagery. Distinguished from Xlg in McCullough Range by distinct equigranular character and abundance of K-feldspar as a prominent phase, making this unit more of granitic than a tonalitic leucogranite. Unit is commonly lineated and sheared with top-east kinematics.

**Xbkg Biotite K-feldspar orthogneiss** Dark brown and gray, strongly porphyritic, biotite granitic orthogneiss. Strongly to moderately foliated and lineated. Large K-feldspar phenocrysts up to ~5 cm in length, but commonly ~2 cm in length. Biotite-rich matrix, and unit varies from coarse- to medium-grained. K-feldspar porphyroclasts are commonly anhedral, rounded, and sheared due to dynamic recrystallization. Relatively fine grain size of all phases due to grain-size reduction during mylonitization. Correlative with the granodiorite of Big Tiger Wash of Miller and Wooden (1993) to the southeast of the study area. Composition is very similar to Xbbp—with prominent K-feldspar porphyroclasts in a dark, bt-rich matrix—but Xbkg is distinguished by a combination of less porphyroclasts, more rounded to sheared-mantled K-feldspar porphyroclasts (sigma and delta clastics due to dynamic recrystallization), and mylonitic texture (reduced grain size of some to all phases). Shear sense is top-east-southeast.

Wooden and Miller (1990) reported a ca. 1.68 Ga age. New geochronology from the McCullough Mountain quadrangle (Zuza et al., 2022) to the east yielded U-Pb zircon ages of ca. 1.66–1.67 Ga (samples MRI20SD-19, MPAZ21-S3, and MPAZ21-S34; table 2). These ages overlap updated age constraints for the Beer Bottle Pass pluton (between ca. 1.66 and 1.69 Ga; Almeida et al., 2016; this study; table 2), suggesting the potassic intrusions are generally of this age.

Regional top-east deformation continued after the crystallization of this unit, and thus deformation was active after ca. 1.66 Ga. The undeformed to less deformed Xg and Xgr units in the McCullough Mountain quadrangle to the east (Zuza et al., 2022) have ages of ca. 1.64 Ga (table 2). Therefore, the observed top-east-southeast deformation is bracketed between ca. 1.66 and 1.64 Ga. This deformation corresponds to the Ivanpah orogeny of Wooden and Miller (1990), which may correlate to the broader Yavapai orogeny (Whitmeyer and Karlstrom, 2007). However, Yavapai deformation has been bracketed to ca. 1.71–1.69 Ga as

observed in the Grand Canyon to the east (Holland et al., 2015). The relationships between phases of Paleoproterozoic deformation requires further attention.

**Xog Orthogneiss, undivided** Heterogeneous orthogneiss, with K-feldspar-rich (syenite) pegmatite bands, equigranular granite bodies, and coarse leucogranite. Minor amphibolite pods. A coarse, undeformed K-feldspar-rich pegmatite within the unit yielded a new U-Pb age of  $1660 \pm 15$  Ma and another pegmatite body yielded a significantly younger age of  $1622 \pm 24$  Ma (samples MPAZ21-S26 and MPAZ21-S17; fig. 3; tables 2 and 4). These ages may bracket deformation, but we cautiously interpret this as a younger bound on deformation because the syenite, pegmatite character of the dated dikes may have resisted deformation while strain was partitioned into more quartz- or mica-rich units.

**Xmg Migmatite gneiss** Dark, coarse-grained lineated schistose biotite migmatite gneiss with complex folding, contains local pods of amphibolite. Commonly garnet bearing and intruded by leucogranite. Mineral assemblage includes garnet + sillimanite + cordierite + biotite + K-feldspar for the pelites and clinopyroxene + orthopyroxene + cummingtonite in the amphibolites. Thermobarometry confirms upper amphibolite-granulite-grade metamorphic conditions at temperatures of  $\sim 700^\circ\text{C}$  and pressures of 3–4 kbar (Young et al., 1989). Miller and Wooden (1988) suggest metamorphism occurred during Ivanpah orogeny at ca. 1.71–1.70 Ga. The protolith age is unknown, but the unit is intruded by all orthogneiss in this study area, and augen gneiss dikes dated to ca. 1.73 Ga (Wooden and Miller, 1990).

## ACKNOWLEDGMENTS

Research supported by the U.S. Geological Survey Earth Mapping Resource Initiative (Earth MRI), (Cooperative Agreement G19AC00255). The views and conclusions contained in this document are those of the authors and should not be interpreted as necessarily representing the official policies, either expressed or implied, of the U.S. Government. We thank David Miller for showing us the geology, sharing notes, and discussion.

## REFERENCES

- Almeida, R.V., Cai, Y., Hemming, S.R., Christie-Blick, N., and Neiswanger, L.S., 2016, Reexamination of the crustal boundary context of Mesoproterozoic granites in southern Nevada using U-Pb zircon chronology and Nd and Pb isotopic compositions: *The Journal of Geology*, v. 124, no. 3, p. 313–329.
- Anderson, R.E., 1971, Thin skin distension in Tertiary rocks of southeastern Nevada: *Geological Society of America Bulletin*, v. 82, p. 43–58.
- Cox, K.G., Bell, J.D., and Pankhurst, R.J., 1979, *The interpretation of igneous rocks*: Allen & Unwin, London.
- Denton, K.M., and Ponce, D.A., 2018, Gravity and magnetic studies of the eastern Mojave Desert, California and Nevada (ver 1.1, August 2018): U.S. Geological Survey Open-File Report 2016-1070, 20 p.
- Denton, K.M., Ponce, D.A., Peacock, J.R., and Miller, D.M., 2020, Geophysical characterization of a Proterozoic REE terrane at Mountain Pass, eastern Mojave Desert, California, USA: *Geosphere*, v. 16, no. 1, p. 456–471.
- DeWitt, E., Anderson, J.L., Barton, H.N., Jachens, R.C., Podwysocki, M.H., Brickey, D.W., and Close, T.J., 1989, Mineral resources of the south McCullough Mountains wilderness study area, Clark County, Nevada: U.S. Geological Survey Bulletin 1730.
- Duebendorfer, E.M., and Christensen, C., 1995, Synkinematic (?) intrusion of the “anorogenic” 1425 Ma Beer Bottle Pass pluton, southern Nevada: *Tectonics*, v. 14, no. 1, p. 168–184.
- Faulds, J.E., Olson, E.L., Harlan, S.S., and McIntosh, W.C., 2002, Miocene extension and fault-related folding in the Highland Range, southern Nevada—a three-dimensional perspective: *Journal of Structural Geology*, v. 24, p. 861–886.
- Garside, L., House, P.K., Burchfiel, B.C., Rowland, S.M., and Buck, B.J., 2012, Geologic map of the Jean quadrangle, Clark County, Nevada: Nevada Bureau of Mines and Geology Map 176, 1:24,000 scale, 11 p.
- Gehrels, G.E., Valencia, V.A., and Ruiz, J., 2008, Enhanced precision, accuracy, efficiency, and spatial resolution of U-Pb ages by laser ablation-multicollector-inductively coupled plasma-mass spectrometry: *Geochemistry, Geophysics, Geosystems*, v. 9, no. 3, 13p.
- Hanson, A.D., 2008, Detrital zircon constraints on the Jean conglomerate and Sevier unroofing near Las Vegas: *Geological Society of America Abstracts with Programs*, v. 40, no. 1, p. 56.
- Herrington, J.M., 2000, Evolution of the Kingman arch: University of Nevada, Las Vegas, M.S. thesis, 82 p.
- Holland, M.E., Karlstrom, K.E., Doe, M.F., Gehrels, G.E., Pecha, M., Shufeldt, O.P., Begg, G., Griffin, W.L., and Belousova, E., 2015, An imbricate midcrustal suture zone—the Mojave-Yavapai province boundary in Grand Canyon, Arizona: *Geological Society of America*, v. 127, no. 9-10, p. 1391–1410.
- House, P.K., Ramelli, A.R., and Buck, B.J., 2006, Surficial geologic map of the Ivanpah Valley area, Clark County, Nevada: Nevada Bureau of Mines and Geology Map 156, scale 1:50,000.
- House, P.K., Buck, B.J., and Ramelli, A.R., 2010, Geologic assessment of piedmont and playa flood hazards in the Ivanpah Valley area, Clark County, Nevada: Nevada Bureau of Mines and Geology Report 53.
- Lamb, M.A., Beard, L.S., Dragos, M., Hanson, A.D., Hickson, T.A., Sitton, M., Umhoefer, P.J., Karlstrom, K.E., Dunbar, N., and McIntosh, W., 2018, Provenance and paleogeography of the 25–17 Ma Rainbow Gardens Formation—evidence for tectonic activity at ca. 19 Ma and internal drainage rather than throughgoing paleorivers on the southwestern Colorado Plateau: *Geosphere*, v. 14, no. 4, p. 1592–1617.

- Le Bas, M.J., Le Maitre, R.W., Streckeisen, A., and Zanettin, B., 1986, A chemical classification of volcanic rocks based on the total alkali-silica diagram: *Journal of Petrology*, v. 27, no .3, p. 745–750.
- Mahan, S.A., Miller, D.M., Menges, C.M., and Yount, J.C., 2007, Late Quaternary stratigraphy and luminescence geochronology of the northeastern Mojave Desert: *Quaternary International* 166, p. 61–78.
- McDonald, E.V., McFadden, L.D., and Wells, S.G., 2003, Regional response of alluvial fans to the Pleistocene–Holocene climatic transition, *in* Enzel, Y., Wells, and Lancaster, N., editors, *Paleoenvironments and paleohydrology of the Mojave and Southern Great Basin deserts*: Geological Society of America Special Paper 368, p. 189–205.
- Miller, D.M., and Wooden, J.L., 1988, An Early Proterozoic batholithic belt in the northern New York Mountains area, California and Nevada: Abstracts of the Geological Society of America, v. 20, p. 215.
- Miller, D.M., and Wooden, J.L., 1993, Geologic map of the New York Mountains area, California and Nevada: U.S. Geological Survey Open-File Report 93.
- Miller, D.M., and Wooden, J.L., 1994, Field guide to Proterozoic geology of the New York, Ivanpah, and Providence Mountains, California: U.S. Geological Survey Open-File Report 94.
- Miller, D.M., Schmidt, K.M., Mahan, S.A., McGeehin, J.P., Owen, L.A., Barron, J.A., Lehmkuhl, F., Löhrer, R., 2010, Holocene landscape response to seasonality of storms in the Mojave Desert: *Quaternary International*. 215. P. 45–61.
- Miller, D.M., Langenheim, V.E., Denton, K.M., and Ponce, D.A., 2019, Strike-slip fault interactions at Ivanpah Valley, California and Nevada, *in* Miller, D.M., editor, *Exploring ends of eras in the eastern Mojave Desert: 2019 Desert Symposium Field Guide and Proceedings*, p. 91–97.
- Nakamura, N., 1974, Determination of REE, Ba, Fe, Mg, Na and K in carbonaceous and ordinary chondrites: *Geochimica et Cosmochimica Acta*, v. 38, no. 5, p. 757–775.
- Shand, S.J., 1943, *Eruptive rocks—their genesis, composition, classification, and their relation to ore-deposits with a chapter on meteorites*: John Wiley & Sons, New York.
- Smith, E., Honn, D., and Johnsen, R., 2010, Volcanoes of the McCullough Range, southern Nevada, *in* Umhoefer, P.J., Beard, L.S., and Lamb, M.A., editors., Miocene tectonics of the Lake Mead region, central Basin and Range: Geological Society of America Special Paper 463, p. 203–219.
- Stacey, J.T., and Kramers, J.D., 1975, Approximation of terrestrial lead isotope evolution by a two-stage model: *Earth and Planetary Science Letters*, v. 26, no. 2, p. 207–221.
- Strickland, A., Wooden, J.L., Mattinson, C.G., Ushikubo, T., Miller, D.M., and Valley, J.W., 2013, Proterozoic evolution of the Mojave crustal province as preserved in the Ivanpah Mountains, southeastern California: *Precambrian Research*, v. 224, p. 222–241.
- Whitmeyer, S.J., and Karlstrom, K.E., 2007, Tectonic model for the Proterozoic growth of North America: *Geosphere*, v. 3, no. 4, p. 220–259.
- Wooden, J.L., and Miller, D.M., 1990, Chronologic and isotopic framework for Early Proterozoic crustal evolution in the eastern Mojave Desert region, SE California: *Journal of Geophysical Research: Solid Earth*, v. 95, p. 20133–20146.
- Young, E.D., Anderson, J.L., Clarke, H.S., and Thomas, W.M., 1989, Petrology of biotite-cordierite-garnet gneiss of the McCullough Range, Nevada—I. Evidence for Proterozoic low-pressure fluid-absent granulite grade metamorphism in the southern Cordillera: *Journal of Petrology*, v. 30, no. 1, p. 39–60.
- Zuza, A.V., Darin, M.H., and Dee, S., 2022, Geologic map of the southern half of the McCullough Mountain quadrangle, Clark County, Nevada: Nevada Bureau of Mines and Geology Open-File Report 2022-08, scale 1:24,000, 32 p.

**Suggested citation:**

Darin, M.H., Zuza, A.V., Dee, S., and Johnsen, R.L., 2022, Geologic map of the Nevada part of the Desert quadrangle and adjacent part of the McCullough Mountain quadrangle, Clark County, Nevada: Nevada Bureau of Mines and Geology Open-File Report 2022-07, scale 1:24,000, 37 p.

© Copyright 2022 The University of Nevada, Reno.  
All Rights Reserved.

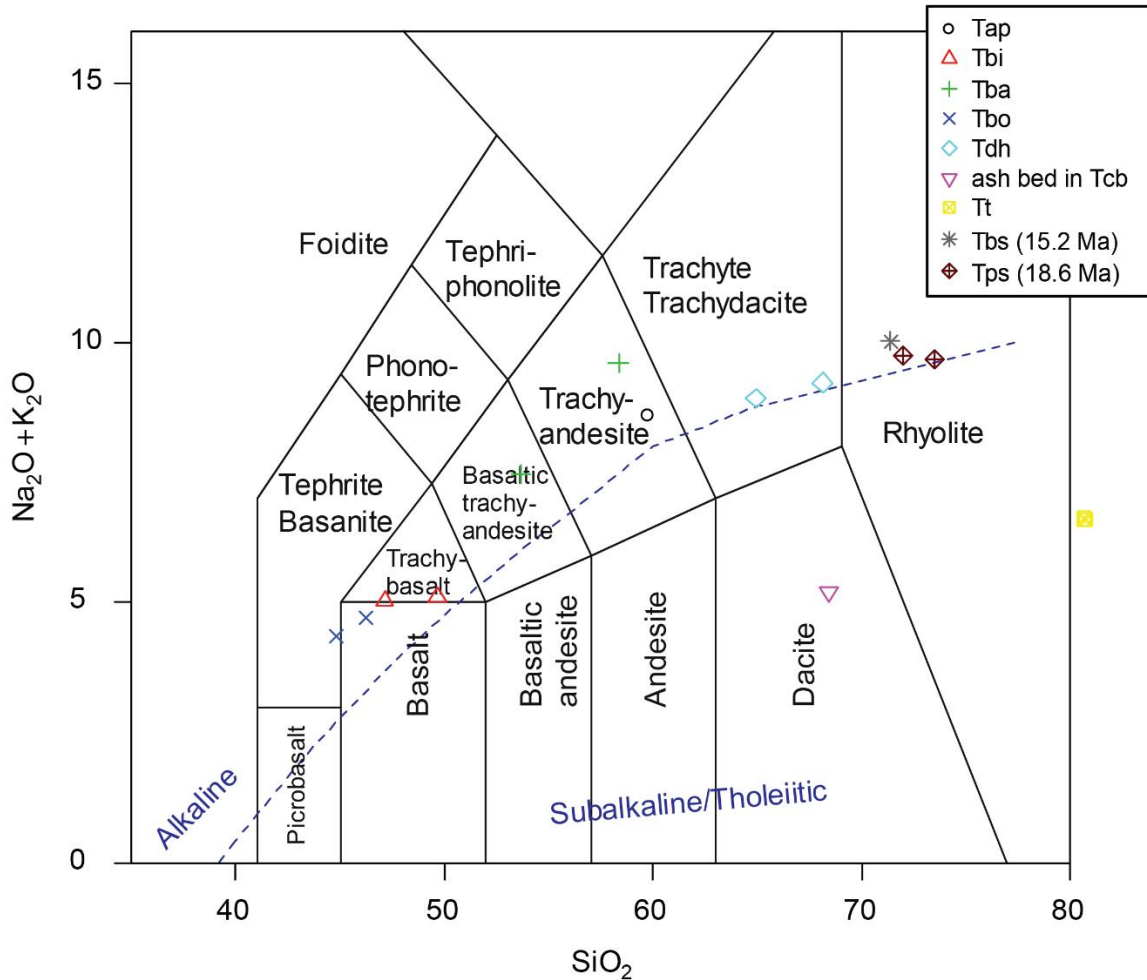


**Figure 1.** Whole-rock geochemical data from the Tertiary volcanic rocks in the study area, plotted as total alkalis ( $\text{Na}_2\text{O} + \text{K}_2\text{O}$ ) versus  $\text{SiO}_2$  (after Le Bas et al., 1986). See table 1 for complete data.

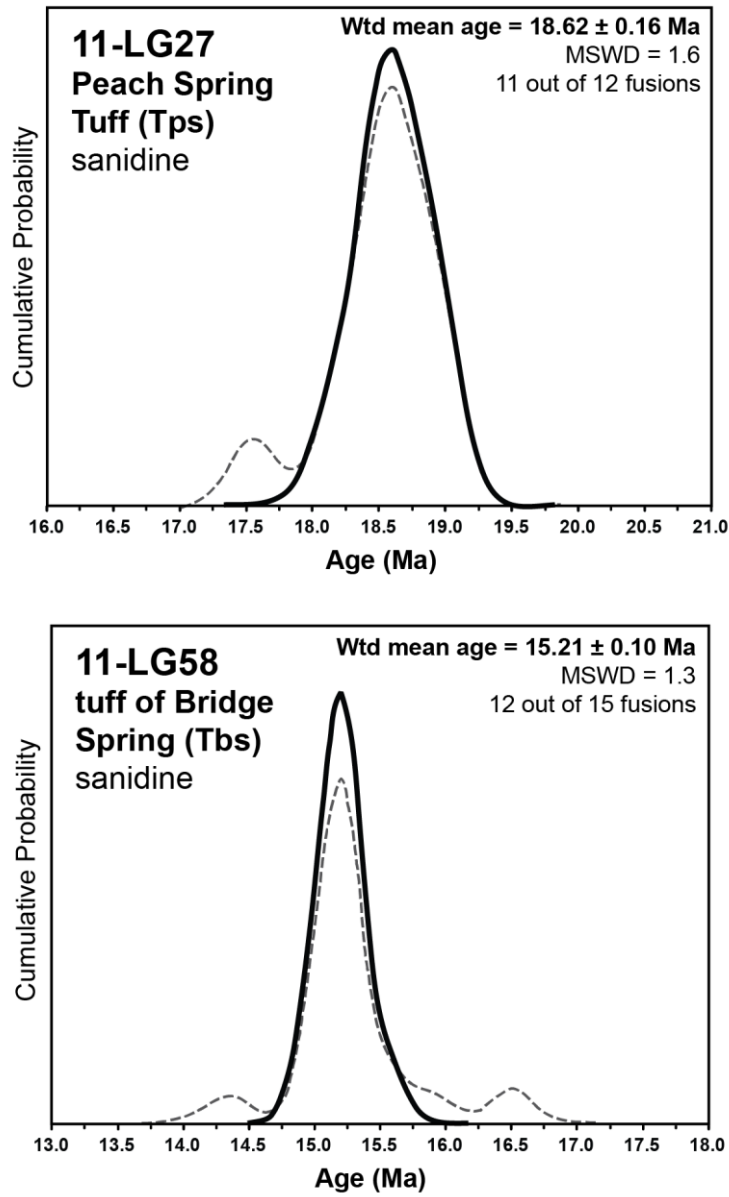


**Figure 2.**  $^{40}\text{Ar}/^{39}\text{Ar}$  data from the study area presented as probability density plots of single-crystal sanidine total fusion ages. Dashed lines represent all analyses and solid lines depict only those analyses used in the weighted mean age calculation. See tables for complete data.

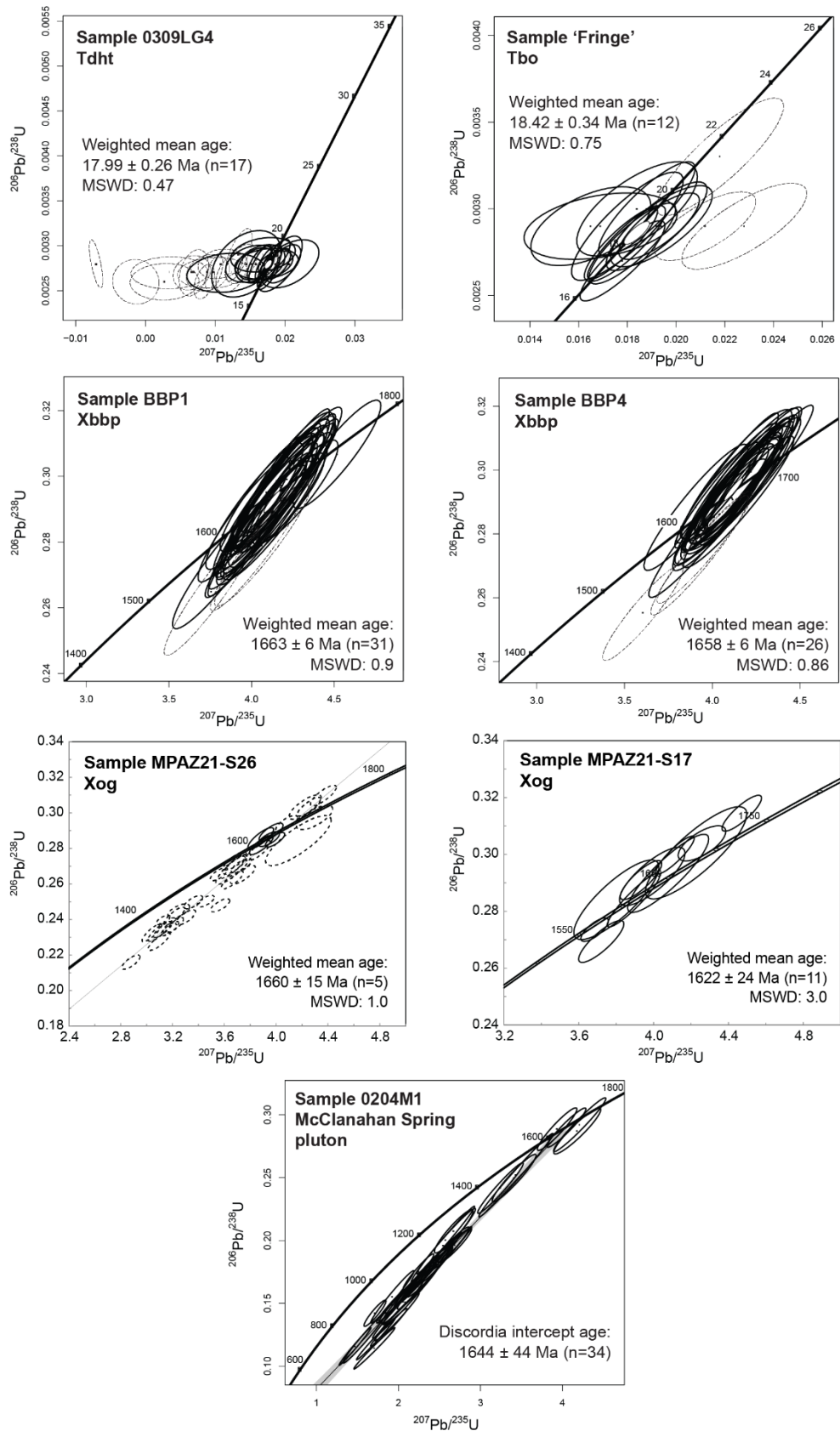


**Figure 3.** Zircon U-Pb results from this study, presented as Wetherill concordia diagrams for each analyzed sample. See Tables 2 and 3 for complete data.

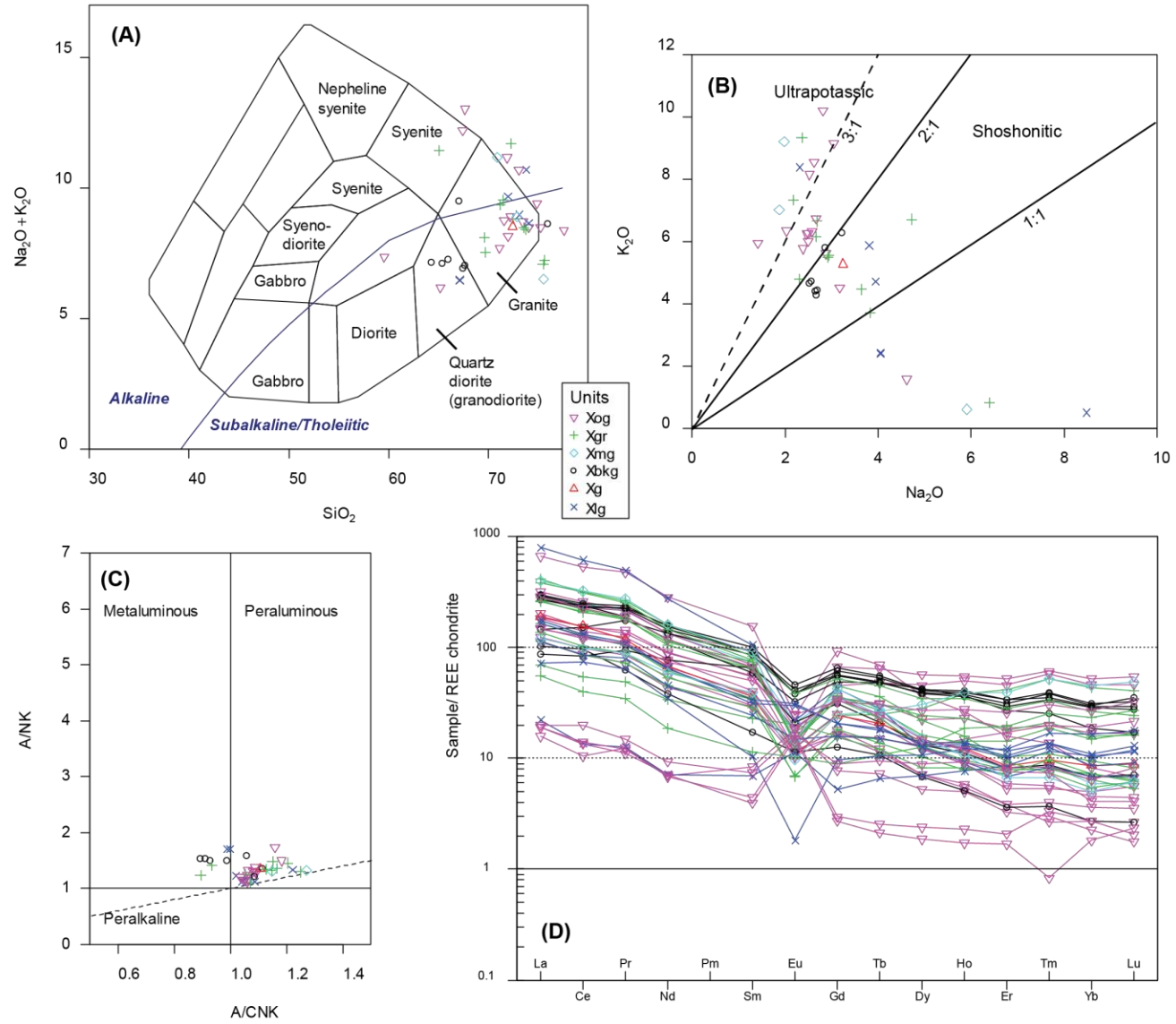


**Figure 4.** Whole-rock geochemical data from Proterozoic orthogneiss units in the study area. (A) Total alkalis ( $\text{Na}_2\text{O} + \text{K}_2\text{O}$ ) versus  $\text{SiO}_2$  (after Cox et al., 1979). (B)  $\text{K}_2\text{O}$  versus  $\text{Na}_2\text{O}$  showing the ultrapotassic-potassic character of most of the Proterozoic rock unit. (C)  $\text{A}/\text{NK}$  versus  $\text{A}/\text{CNK}$  [ $\text{A}/\text{CNK} = \text{molar ratio } \text{Al}_2\text{O}_3/(\text{CaO}+\text{Na}_2\text{O}+\text{K}_2\text{O})$  and  $\text{A}/\text{NK} = \text{molar ratio } \text{Al}_2\text{O}_3/(\text{Na}_2\text{O}+\text{K}_2\text{O})$ ] diagram showing peraluminous character of most of the Proterozoic rock units (after Shand, 1943). (D) Chondrite-normalized rare earth element (REE) diagram (Nakamura, 1974).

**Table 1. Whole-rock geochemical data from Lucy Gray Mountains and the McCullough Range.**

Sample	MPMD21-S4	MP21SD-2	MPAZ21-S41	MPMD21-S11	MPMD21-S14	MPMD21-S10	MPMD21-S16
Unit Name	Tap	Xog	Tbi	Tba	Tba	Tbo	Tbo
Quadrangle	McCullough	Desert	McCullough	Desert	Desert	Desert	Desert
Latitude	35.558479	35.594788	35.508539	35.568381	35.535478	35.57004	35.520518
Longitude	-115.247128	-115.298359	-115.174378	-115.255115	-115.255141	-115.25931	-115.257213
Major elements (wt %)							
SiO <sub>2</sub>	59	46.1	46.7	51.9	57	43.2	43.5
TiO <sub>2</sub>	0.84	3.74	1.32	1.2	0.93	2.13	1.87
Al <sub>2</sub> O <sub>3</sub>	16.4	13.1	15.9	15.9	16.8	11.4	10.6
Fe <sub>2</sub> O <sub>3</sub>	5.16	16.3	8.91	7.13	4.99	10.2	9.57
MnO	0.08	0.3	0.15	0.11	0.08	0.15	0.13
MgO	2.92	5.58	7.42	5.16	3.21	12	11.2
CaO	5.43	6.93	8.28	7.01	4.53	11.7	11.3
Na <sub>2</sub> O	3.94	3.9	2.18	3.91	4.58	3.1	2.2
K <sub>2</sub> O	4.56	1.02	2.63	3.34	4.83	1.09	2.23
P <sub>2</sub> O <sub>5</sub>	0.45	0.85	0.56	1.11	0.77	1.49	1.54
SrO	0.15	<0.01	0.06	0.29	0.18	0.23	0.27
BaO	0.22	0.03	0.09	0.32	0.24	0.25	0.31
V <sub>2</sub> O <sub>5</sub>	0.02	0.06	0.03	0.03	0.02	0.04	0.03
Cr <sub>2</sub> O <sub>3</sub>	0.01	0.01	0.04	<0.01	<0.01	0.07	0.06
LOI*	1.17	2.58	6.22	2.87	1.55	3.75	5.62
Total	100.35	100.5	100.49	100.28	99.71	100.8	100.43
Minor and trace elements (ppm)							
Ag	<1	<1	3	<1	<1	<1	<1
As	10	<5	<5	7	12	5	7
B	26	14	11	12	21	11	<10
Ba	1790	278	669	2520	1920	1870	2450
Be	<5	<5	<5	<5	7	<5	<5
Bi	<0.1	<0.1	<0.1	0.1	<0.1	<0.1	0.1
Cd	<0.2	<0.2	<0.2	<0.2	<0.2	<0.2	<0.2
Ce	194	51.8	73.8	344	271	302	361
Co	18.6	44.9	35.7	26.6	19.3	51.2	47.7
Cr	81	82	266	53	33	475	390
Cs	3.2	<0.1	1.4	9.7	2.3	0.6	1.6
Cu	78	<5	51	76	88	69	77
Dy	4.6	8.41	3.89	6.74	5.36	7.54	8.13
Er	1.83	4.29	2.54	2.59	2	2.82	2.52
Eu	2.52	2.81	1.64	4.9	3.26	5.34	6.41
Ga	23.3	21.4	16.1	23.8	22.8	18	18.5
Gd	8.73	10	5.39	16.8	11.4	16.7	19.6
Ge	1	2	1	1	1	1	1
Hf	9	6	4	11	11	8	9
Ho	0.69	1.77	0.86	1.05	0.89	1.21	1.2
In	<0.2	<0.2	<0.2	<0.2	<0.2	<0.2	<0.2
La	102	21	38.2	171	142	145	177
Li	17	16	62	21	19	13	14
Lu	0.21	0.56	0.37	0.28	0.27	0.33	0.21
Mn	595	2240	1100	861	654	1130	1030
Mo	<2	<2	<2	<2	2	<2	<2
Nb	22.9	20.7	17.5	28.2	34.9	39.7	37.9
Nd	77.8	35.7	34	148	112	144	168
Ni	50	49	124	45	43	336	303
Pb	27	<5	11	36	37	9	15
Pr	22.8	7.42	9.31	42.8	32	39.2	46.6
Rb	125	46.6	221	57	122	28.4	34.2

Sample	MPMD21-S4	MP21SD-2	MPAZ21-S41	MPMD21-S11	MPMD21-S14	MPMD21-S10	MPMD21-S16
Re	<0.02	<0.02	<0.02	<0.02	<0.02	<0.02	<0.02
Sb	0.5	<0.1	<0.1	0.3	0.6	<0.1	0.1
Sc	11	38	26	13	8	21	18
Se	<5	<5	<5	<5	<5	8	<5
Sm	12	10.4	5.7	24	14.9	23.7	29
Sn	<1	1	1	2	1	2	2
Sr	1460	213	575	2590	1690	2150	2350
Ta	1.3	1.4	1.5	1.3	1.6	1.7	1.7
Tb	1.02	1.51	0.78	1.86	1.29	1.93	2.17
Te	<0.5	<0.5	<0.5	<0.5	<0.5	<0.5	<0.5
Th	31.1	1.8	5.6	28.7	33.1	11.3	16
Tl	<0.5	<0.5	1.2	<0.5	<0.5	<0.5	<0.5
Tm	0.28	0.58	0.35	0.35	0.25	0.35	0.28
U	6.74	0.84	2.84	4.75	7.12	3.11	3.29
V	105	348	186	176	119	199	131
W	2	<1	<1	<1	2	<1	<1
Y	20.8	42.2	23.3	29.5	22.2	31.8	30.5
Yb	1.6	3.5	2.4	2	1.7	1.9	1.9
Zn	65	162	90	98	76	118	118
Zr	374	235	157	469	528	395	415

**Table 1. Whole-rock geochemical data from Lucy Gray Mountains and the McCullough Range (continued).**

Sample	MPMD21-S15	MPMD21-S1	MP21SD-1	MPAZ21-S40D	MPAZ21-S40	MPMD21-S3	MPMD21-S12
UnitName	Tdh	Tdh	Tcb	Tt	Tt	Tbs	Tps
Quadrangle	Desert	McCullough	Desert	McCullough	McCullough	McCullough	Desert
Latitude	35.51976	35.54888	35.528485	35.516212	35.516212	35.55762	35.576174
Longitude	-115.258674	-115.15204	-115.259812	-115.162464	-115.162464	-115.244266	-115.256449
Major elements (wt%)							
SiO <sub>2</sub>	66.6	62.8	56.8	80.1	79.2	70.6	70.7
TiO <sub>2</sub>	0.33	0.62	0.14	0.04	0.04	0.35	0.28
Al <sub>2</sub> O <sub>3</sub>	16.2	16.7	11	11.1	11	14.4	13.4
Fe <sub>2</sub> O <sub>3</sub>	2.4	4.03	0.93	0.44	0.45	1.65	1.52
MnO	0.05	0.06	0.05	0.03	0.03	0.07	0.07
MgO	0.65	1.15	9.01	0.23	0.24	0.37	0.43
CaO	2.38	2.4	0.77	0.71	0.72	1.49	2.16
Na <sub>2</sub> O	4.49	3.62	3.42	2.92	2.89	4.12	3.19
K <sub>2</sub> O	4.55	5.02	0.9	3.62	3.61	5.81	6.39
P <sub>2</sub> O <sub>5</sub>	0.13	0.34	0.03	<0.01	<0.01	0.05	0.05
SrO	0.16	0.15	0.2	0.01	0.01	<0.01	0.01
BaO	0.26	0.22	0.04	0.02	0.03	0.02	0.04
V <sub>2</sub> O <sub>5</sub>	<0.01	0.02	<0.01	<0.01	<0.01	<0.01	<0.01
Cr <sub>2</sub> O <sub>3</sub>	<0.01	<0.01	<0.01	<0.01	0.02	<0.01	0.06
LOI*	0.88	2.97	15.4	1.66	1.56	1	1.99
Total	99.08	100.1	98.69	100.88	99.8	99.93	100.29
Minor and trace elements (ppm)							
Ag	<1	<1	<1	<1	3	<1	2
As	<5	<5	<5	<5	<5	7	7
B	18	15	29	<10	<10	40	13
Ba	2140	1950	382	284	278	134	201
Be	<5	<5	<5	<5	<5	8	<5
Bi	<0.1	<0.1	0.1	0.1	0.1	<0.1	0.1
Cd	0.2	<0.2	<0.2	<0.2	<0.2	<0.2	<0.2
Ce	153	164	47.4	15.2	15.1	183	174
Co	3.2	9.5	1	<0.5	<0.5	1.8	2.1
Cr	<10	15	<10	<10	<10	15	13
Cs	1.3	0.9	1	2.3	1.9	3	0.6
Cu	<5	14	<5	<5	<5	<5	<5
Dy	2.7	3.79	1.43	1.87	1.87	6.46	7.65
Er	1.26	1.72	0.75	0.93	0.9	3.89	3.85
Eu	1.53	2.47	0.27	0.36	0.39	0.91	1.27
Ga	19.8	23.2	12	15.8	16.9	19.9	18
Gd	5.39	7.18	2.03	1.8	1.85	8.96	8.95
Ge	1	1	<1	1	1	1	1
Hf	8	8	3	2	2	11	9
Ho	0.43	0.67	0.21	0.38	0.37	1.39	1.43
In	<0.2	<0.2	<0.2	<0.2	<0.2	<0.2	<0.2
La	81.2	85.8	24.7	6.5	7.2	89.9	88.4
Li	10	<10	62	<10	<10	23	27
Lu	0.17	0.25	0.11	0.17	0.13	0.45	0.48
Mn	362	478	382	175	179	538	530
Mo	<2	<2	<2	<2	<2	<2	<2
Nb	16.1	14.9	10.9	19.7	20.5	48.8	34.5
Nd	56.3	66.4	17.3	7.2	6.8	67.7	65.1
Ni	11	20	8	15	11	25	25
Pb	34	33	11	31	34	39	31
Pr	17.5	19.4	5.37	1.83	1.65	21	20.2
Rb	83.1	90.9	26.9	93	97.1	202	155

Sample	MPMD21-S15	MPMD21-S1	MP21SD-1	MPAZ21-S40D	MPAZ21-S40	MPMD21-S3	MPMD21-S12
Re	<0.02	<0.02	<0.02	<0.02	<0.02	<0.02	<0.02
Sb	0.2	0.4	0.1	0.4	0.5	0.7	0.5
Sc	<5	6	<5	<5	<5	<5	<5
Se	<5	<5	<5	<5	5	<5	9
Sm	8.9	10	3.1	1.8	2.4	13.3	11.2
Sn	2	1	<1	1	<1	2	4
Sr	1510	1400	1830	198	199	91.6	148
Ta	0.7	0.6	0.8	1.2	1.2	2.7	2
Tb	0.61	0.84	0.26	0.29	0.3	1.28	1.32
Te	<0.5	<0.5	<0.5	<0.5	<0.5	<0.5	<0.5
Th	20	17	10.1	8.7	8.7	46	30.4
Tl	<0.5	<0.5	<0.5	0.6	0.7	0.9	<0.5
Tm	0.16	0.23	0.12	0.16	0.13	0.58	0.55
U	3.46	3.11	3.46	1.23	1.26	7.83	2.46
V	27	70	16	<5	<5	14	8
W	<1	<1	<1	<1	2	2	<1
Y	13.3	17.9	9	10.3	10.8	36.1	38.8
Yb	0.9	1.7	0.8	0.9	0.9	3.6	3.8
Zn	48	65	49	17	18	37	44
Zr	298	308	105	43.4	43.3	377	305

**Table 1. Whole-rock geochemical data from Lucy Gray Mountains and the McCullough Range (continued).**

Sample	MPMD21-S13	MPAZ21-S1	MPAZ21-S5	MPAZ21-S9	MPAZ21-S10	MPAZ21-S33dup	MPAZ21-S33
UnitName	Tps	Xbkg	Xbkg	Xbkg	Xbkg	Xbkg	Xbkg
Quadrangle	Desert	McCullough	McCullough	McCullough	McCullough	McCullough	McCullough
Latitude	35.592258	35.500767	35.530836	35.517875	35.526755	35.504186	35.504186
Longitude	-115.250825	-115.158616	-115.159834	-115.143829	-115.15492	-115.184122	-115.184122
Major elements (wt %)							
SiO <sub>2</sub>	72	65.2	75.5	66.3	66.6	63.5	64.9
TiO <sub>2</sub>	0.26	1.09	0.14	0.57	1.03	1.25	1.17
Al <sub>2</sub> O <sub>3</sub>	13.4	13.8	13.2	16.1	13.5	13.9	14.1
Fe <sub>2</sub> O <sub>3</sub>	1.38	6.44	0.84	3.9	6.04	7.22	6.63
MnO	0.05	0.11	0.01	0.04	0.08	0.12	0.11
MgO	0.24	1.26	0.25	0.65	1.04	1.42	1.25
CaO	1.16	3.12	0.69	1.39	2.6	3.58	3.48
Na <sub>2</sub> O	3.63	2.52	2.83	3.17	2.6	2.48	2.66
K <sub>2</sub> O	5.86	4.67	5.76	6.21	4.33	4.6	4.41
P <sub>2</sub> O <sub>5</sub>	0.03	0.45	0.05	0.3	0.42	0.54	0.45
SrO	<0.01	0.02	<0.01	0.02	0.02	0.03	0.03
BaO	0.02	0.17	0.14	0.19	0.17	0.18	0.18
V <sub>2</sub> O <sub>5</sub>	<0.01	0.01	<0.01	<0.01	<0.01	0.01	<0.01
Cr <sub>2</sub> O <sub>3</sub>	<0.01	<0.01	<0.01	<0.01	<0.01	<0.01	<0.01
LOI*	1.12	1.04	0.66	1.37	1.29	0.86	0.73
Total	99.15	99.9	100.07	100.21	99.72	99.69	100.1
Minor and trace elements (ppm)							
Ag	2	<1	<1	<1	<1	<1	<1
As	6	<5	<5	<5	<5	<5	<5
B	18	<10	<10	10	<10	<10	<10
Ba	85.1	1370	1140	1540	1320	1370	1390
Be	<5	<5	<5	<5	<5	<5	<5
Bi	<0.1	<0.1	<0.1	0.2	0.3	0.1	<0.1
Cd	<0.2	<0.2	<0.2	<0.2	<0.2	<0.2	0.2
Ce	157	130	84	205	208	200	216
Co	1.1	10	1.6	6	5.8	10.5	9.3
Cr	<10	33	12	29	17	14	25
Cs	1.5	2.5	1	3.4	1.1	2.8	2.4
Cu	<5	10	<5	35	11	7	11
Dy	7.56	14	2.35	4.53	13.5	14.2	13.2
Er	4.18	7.66	0.81	1.84	7.06	7.63	6.54
Eu	0.86	2.98	0.88	1.62	2.98	3.53	3.18
Ga	18.8	22.6	17.8	23.2	22.1	23.4	23
Gd	9.44	16.8	3.5	8.6	15.4	17.9	15.5
Ge	2	2	2	2	2	2	2
Hf	9	15	5	9	16	17	14
Ho	1.36	2.72	0.36	0.78	2.61	2.86	2.52
In	<0.2	<0.2	<0.2	<0.2	<0.2	0.2	<0.2
La	77.5	48.4	34	89.7	97.6	88.8	99.3
Li	20	22	<10	10	11	24	22
Lu	0.49	0.99	0.09	0.24	1.19	1.11	0.93
Mn	414	802	60	277	573	877	847
Mo	<2	3	<2	4	<2	<2	2
Nb	39.7	35.1	7.5	16.7	32.2	42.4	37.7
Nd	61.5	84.8	24	74.4	92.1	99	98.4
Ni	18	18	12	14	15	10	18
Pb	58	27	30	61	27	28	29
Pr	18.9	19.7	7.06	21.1	25	25.6	26.7
Rb	206	198	258	251	150	215	199

Sample	MPMD21-S13	MPAZ21-S1	MPAZ21-S5	MPAZ21-S9	MPAZ21-S10	MPAZ21-S33dup	MPAZ21-S33
Re	<0.02	<0.02	<0.02	<0.02	0.2	<0.02	<0.02
Sb	0.4	<0.1	<0.1	<0.1	<0.1	<0.1	<0.1
Sc	<5	18	<5	8	15	19	18
Se	7	<5	<5	<5	<5	<5	<5
Sm	12	17.4	3.5	11.9	18.9	20.6	18.6
Sn	2	4	2	3	3	5	4
Sr	37.7	274	122	222	257	289	318
Ta	2.2	2.3	<0.5	1	1.9	2.6	2.4
Tb	1.39	2.52	0.5	1	2.24	2.6	2.32
Te	<0.5	<0.5	<0.5	<0.5	<0.5	<0.5	<0.5
Th	30.9	4.9	24.3	48.8	14.3	15.4	17.1
Tl	0.8	1.1	1.3	1.4	1	1.2	1.1
Tm	0.53	1.06	0.11	0.26	1.16	1.17	1.01
U	4.22	2.62	2.37	2.77	1.97	2.41	2.15
V	9	54	5	32	43	53	52
W	1	<1	<1	<1	<1	<1	<1
Y	35.5	69.6	9.9	16.9	62.5	78.4	67.2
Yb	3.5	6.5	0.6	1.5	6.6	6.8	6.3
Zn	50	114	16	78	115	118	110
Zr	301	571	160	297	671	775	622

**Table 1. Whole-rock geochemical data from Lucy Gray Mountains and the McCullough Range (continued).**

Sample	MRI20SD-19	MPAZ21-S29	MPAZ21-S3	MPAZ21-S13	MPAZ21-S31	MPAZ21-S4	MPAZ21-S11
UnitName	Xbkg	Xg	Xgr	Xgr	Xgr	Xgr	Xgr
Quadrangle	Crescent Peak	McCullough	McCullough	McCullough	McCullough	McCullough	McCullough
Latitude	35.491275	35.560187	35.525436	35.530313	35.561233	35.525798	35.528364
Longitude	-115.160732	-115.140646	-115.153042	-115.169513	-115.164219	-115.151948	-115.164307
Major elements (wt %)							
SiO <sub>2</sub>	66.5	71.6	62.7	72.3	74.8	69	68.4
TiO <sub>2</sub>	0.94	0.25	0.54	0.02	0.21	1.05	0.51
Al <sub>2</sub> O <sub>3</sub>	14.1	14.7	17.9	14.9	12.9	14.3	15.7
Fe <sub>2</sub> O <sub>3</sub>	6.02	2.08	0.63	2.2	2.43	2.4	3.18
MnO	0.07	0.03	<0.01	0.11	0.05	0.02	0.03
MgO	1.08	0.34	0.16	0.29	0.52	1.4	0.69
CaO	2.45	1.3	3.04	0.97	1.01	2.81	1.66
Na <sub>2</sub> O	2.62	3.21	4.55	2.65	2.28	3.79	3.58
K <sub>2</sub> O	4.21	5.21	6.47	6.14	4.74	3.66	4.38
P <sub>2</sub> O <sub>5</sub>	0.51	0.07	0.29	0.07	0.05	0.42	0.06
SrO	<0.01	0.01	<0.01	<0.01	<0.01	0.03	<0.01
BaO	0.12	0.06	0.12	0.12	0.1	0.14	0.1
V <sub>2</sub> O <sub>5</sub>	<0.01	<0.01	<0.01	<0.01	<0.01	<0.01	<0.01
Cr <sub>2</sub> O <sub>3</sub>	<0.01	<0.01	<0.01	<0.01	<0.01	<0.01	<0.01
LOI*	1.25	1.12	3.2	0.77	0.94	1.31	1.24
Total	99.87	99.98	99.6	100.54	100.03	100.33	99.53
Minor and trace elements (ppm)							
Ag	<1	<1	<1	<1	<1	<1	<1
As	<5	<5	<5	<5	<5	<5	<5
B	<10	<10	<10	<10	<10	<10	<10
Ba	1060	421	1120	1060	806	1030	689
Be	<5	<5	<5	<5	<5	<5	<5
Bi	<0.1	<0.1	<0.1	<0.1	<0.1	<0.1	<0.1
Cd	<0.2	<0.2	<0.2	<0.2	<0.2	<0.2	<0.2
Ce	71.7	135	47.3	112	190	275	268
Co	8.4	2.9	<0.5	1.9	5.2	2.3	5.1
Cr	18	18	17	20	21	22	34
Cs	2.9	2.6	1	1.6	0.6	0.4	0.6
Cu	18	<5	<5	5	<5	<5	<5
Dy	14.5	4.95	4.49	9.71	8.44	11.8	7.52
Er	6.09	1.94	3.22	9.44	4.07	6.28	2.07
Eu	2.5	0.8	1.55	0.95	1.31	2.96	1.04
Ga	25.8	21.6	17.5	15.3	16.6	17.7	26.6
Gd	13.5	6.74	4.37	6.7	9.8	14.4	12.4
Ge	2	2	1	2	2	2	2
Hf	15	7	13	4	10	16	11
Ho	2.6	0.87	1	2.71	1.61	2.42	1.1
In	<0.2	<0.2	<0.2	<0.2	<0.2	<0.2	<0.2
La	28.9	62.3	23.1	54.8	93	126	137
Li	16	14	<10	<10	<10	<10	11
Lu	0.58	0.3	0.57	1.39	0.55	0.83	0.21
Mn	540	183	41	828	356	144	196
Mo	2	<2	<2	<2	<2	<2	<2
Nb	52.5	13.4	14.4	0.6	8.2	32.8	21.7
Nd	48.7	42.9	21.2	39	66.7	101	92.7
Ni	16	18	9	14	16	13	17
Pb	17	39	14	39	38	14	44
Pr	10.5	13.2	5.49	11.8	20.6	29.3	28.3
Rb	303	267	226	199	159	101	175

Sample	MRI20SD-19	MPAZ21-S29	MPAZ21-S3	MPAZ21-S13	MPAZ21-S31	MPAZ21-S4	MPAZ21-S11
Re	<0.02	<0.02	<0.02	<0.02	<0.02	<0.02	<0.02
Sb	<0.1	<0.1	<0.1	<0.1	<0.1	<0.1	<0.1
Sc	13	<5	<5	10	6	13	<5
Se	<5	<5	<5	<5	<5	<5	<5
Sm	13.3	7.3	4.7	7	12.9	17.1	15.8
Sn	3	3	3	1	1	5	3
Sr	210	98.1	150	149	134	271	113
Ta	2.1	0.8	0.7	<0.5	<0.5	2	1
Tb	2.27	0.98	0.7	1.18	1.44	2.14	1.69
Te	<0.5	<0.5	<0.5	<0.5	<0.5	<0.5	<0.5
Th	3.4	44.8	10	28.4	54.2	28.2	66.6
Tl	1.7	1.6	1	1.1	0.8	0.5	0.9
Tm	0.77	0.29	0.56	1.57	0.63	0.99	0.22
U	2.16	3.14	2.88	3.86	4.87	2.83	7.05
V	46	13	22	<5	15	35	29
W	<1	<1	<1	<1	<1	<1	<1
Y	69.7	16.6	30.7	72.8	42.2	56.7	29.4
Yb	4.1	1.9	3.3	9.5	3.5	5.8	1.2
Zn	115	45	<5	12	20	12	55
Zr	684	227	452	118	357	698	491

**Table 1. Whole-rock geochemical data from Lucy Gray Mountains and the McCullough Range (continued).**

Sample	MPAZ21-S30	MPAZ21-S32	MPMD21-S6	MPMD21-S7	MPMD21-S6D	AZ4-14-21(1)	MPAZ21-S2
UnitName	Xgr	Xgr	Xgr	Xgr	Xgr	Xgr	Xlg
Quadrangle	McCullough	McCullough	McCullough	McCullough	McCullough	Desert	McCullough
Latitude	35.56106	35.556357	35.543087	35.550564	35.543087	35.540267	35.516308
Longitude	-115.149529	-115.174445	-115.195222	-115.188907	-115.195222	-115.268656	-115.154127
Major elements (wt %)							
SiO <sub>2</sub>	70.6	72	73.6	75.2	73.9	70.6	65.9
TiO <sub>2</sub>	0.25	<0.01	0.14	0.01	0.15	0.31	0.75
Al <sub>2</sub> O <sub>3</sub>	15.2	15.4	14.5	14.7	14.4	14.3	15.5
Fe <sub>2</sub> O <sub>3</sub>	2.28	0.09	1.73	0.82	1.7	2.23	4.24
MnO	0.03	<0.01	0.05	0.02	0.05	0.02	0.03
MgO	0.47	0.01	0.34	1.2	0.33	0.48	1.69
CaO	0.94	0.24	1.1	0.22	1.09	1.2	3.54
Na <sub>2</sub> O	2.67	2.35	2.95	6.36	2.93	2.16	3.98
K <sub>2</sub> O	6.6	9.31	5.55	0.82	5.5	7.25	2.35
P <sub>2</sub> O <sub>5</sub>	0.09	0.12	0.07	0.05	0.07	0.14	0.07
SrO	0.01	<0.01	<0.01	<0.01	<0.01	0.02	0.03
BaO	0.09	0.12	0.07	<0.01	0.08	0.1	0.08
V <sub>2</sub> O <sub>5</sub>	<0.01	<0.01	<0.01	<0.01	<0.01	<0.01	0.01
Cr <sub>2</sub> O <sub>3</sub>	<0.01	<0.01	0.01	<0.01	<0.01	<0.01	<0.01
LOI*	0.96	0.46	0.65	1.29	0.49	0.73	1.7
Total	100.19	100.1	100.76	100.69	100.69	99.54	99.87
Minor and trace elements (ppm)							
Ag	<1	<1	<1	<1	<1	1	<1
As	<5	<5	<5	<5	<5	<5	<5
B	<10	<10	<10	<10	<10	<10	<10
Ba	570	1130	622	36.1	623	813	771
Be	<5	<5	<5	<5	<5	<5	<5
Bi	<0.1	<0.1	<0.1	<0.1	<0.1	<0.1	0.2
Cd	<0.2	<0.2	<0.2	<0.2	<0.2	<0.2	<0.2
Ce	182	6.7	73.8	34.6	89.6	180	109
Co	4.1	<0.5	1.9	1.2	2.1	3.1	4.4
Cr	27	16	<10	<10	<10	<10	45
Cs	2.1	2.5	0.8	0.2	1.5	0.8	0.3
Cu	<5	<5	<5	<5	<5	<5	<5
Dy	5.51	0.27	2.84	4.3	3.54	4.45	4.8
Er	2.32	0.15	1.64	4.4	1.77	1.77	2.61
Eu	1.11	1.38	0.54	0.8	0.53	1.09	2.42
Ga	19.4	13.9	16.2	16.2	15.9	17.9	24.1
Gd	10.1	0.3	4.25	2.47	5.07	9.35	5.7
Ge	2	2	2	1	2	1	2
Hf	6	<1	4	4	4	12	10
Ho	0.97	<0.05	0.57	1.32	0.55	0.68	0.96
In	<0.2	<0.2	<0.2	<0.2	<0.2	<0.2	0.2
La	84.8	5.4	37.9	18.2	45.5	87.9	54.9
Li	18	<10	<10	<10	<10	<10	17
Lu	0.28	<0.05	0.21	0.91	0.18	0.22	0.4
Mn	222	19	365	129	356	183	207
Mo	<2	<2	<2	<2	<2	<2	3
Nb	10	0.3	7.7	0.4	7.9	15.3	24.2
Nd	70.6	2.2	28.3	11.8	33.6	73.3	40.5
Ni	20	19	11	11	12	13	29
Pb	47	54	34	<5	35	37	9
Pr	20.2	0.68	8.15	3.9	9.87	21.5	12.1
Rb	267	323	205	35.5	211	238	70.4

Sample	MPAZ21-S30	MPAZ21-S32	MPMD21-S6	MPMD21-S7	MPMD21-S6D	AZ4-14-21(1)	MPAZ21-S2
Re	<0.02	<0.02	<0.02	<0.02	<0.02	<0.02	<0.02
Sb	<0.1	<0.1	<0.1	<0.1	<0.1	<0.1	<0.1
Sc	5	<5	<5	7	<5	<5	9
Se	<5	<5	5	5	6	<5	<5
Sm	15	0.1	5.8	2.3	6.9	13.2	6.9
Sn	3	2	1	<1	<1	1	4
Sr	146	130	120	36.8	121	159	277
Ta	0.8	<0.5	<0.5	<0.5	<0.5	<0.5	1.5
Tb	1.26	<0.05	0.57	0.5	0.64	1.07	0.85
Te	<0.5	<0.5	<0.5	<0.5	<0.5	<0.5	<0.5
Th	53.1	1.1	21.2	8.6	24.9	69.5	10.4
Tl	1.5	1.8	1	<0.5	1.1	1.2	<0.5
Tm	0.33	<0.05	0.29	0.77	0.24	0.24	0.41
U	6.9	0.21	3.32	1.81	3.86	5.29	4.24
V	12	<5	9	<5	9	15	47
W	<1	<1	<1	<1	<1	<1	<1
Y	25.8	1.2	16.5	36.6	17	19.4	20.8
Yb	2.1	0.1	1.6	5.2	1.4	1.6	2.2
Zn	36	<5	24	<5	23	50	7
Zr	217	2.8	117	144	115	374	349

**Table 1. Whole-rock geochemical data from Lucy Gray Mountains and the McCullough Range (continued).**

Sample	MPAZ21-S6	MPAZ21-S7	MPAZ21-S8	MPAZ21-S2dup	D01	MPAZ21-S19	MRI20SD-38
UnitName	Xlg	Xlg	Xlg	Xlg	Xeg?	Xog?	Xmg
Quadrangle	McCullough	McCullough	McCullough	McCullough	Desert	Desert	Hopps Well
Latitude	35.53105	35.528066	35.507818	35.516308	35.597263	35.542743	35.386726
Longitude	-115.14929	-115.140449	-115.126521	-115.154127	-115.253351	-115.279369	-115.117831
Major elements (wt %)							
SiO <sub>2</sub>	72.4	73.7	71.6	65.8	73.3	70.6	72.4
TiO <sub>2</sub>	0.25	0.07	0.29	0.72	0.01	0.27	0.32
Al <sub>2</sub> O <sub>3</sub>	16	15.4	15.3	15.5	14.4	14.8	13.8
Fe <sub>2</sub> O <sub>3</sub>	0.98	0.92	1.02	4.19	0.31	1.72	2.62
MnO	0.01	0.02	<0.01	0.03	0.03	0.02	0.01
MgO	0.17	0.12	0.06	1.64	0.04	0.36	0.45
CaO	0.22	0.59	1.35	3.61	0.55	0.46	0.78
Na <sub>2</sub> O	8.39	3.92	3.79	3.98	2.3	1.97	1.86
K <sub>2</sub> O	0.49	4.69	5.84	2.36	8.33	9.17	6.97
P <sub>2</sub> O <sub>5</sub>	0.05	0.09	0.1	0.07	0.08	0.1	0.1
SrO	<0.01	<0.01	0.01	0.03	<0.01	0.01	<0.01
BaO	0.05	0.01	0.11	0.09	0.01	0.16	0.1
V <sub>2</sub> O <sub>5</sub>	<0.01	<0.01	<0.01	<0.01	<0.01	<0.01	<0.01
Cr <sub>2</sub> O <sub>3</sub>	<0.01	<0.01	<0.01	<0.01	<0.01	<0.01	<0.01
LOI*	1.04	0.91	0.82	1.6	0.33	0.51	0.93
Total	100.05	100.44	100.29	99.62	99.69	100.15	100.34
Minor and trace elements (ppm)							
Ag	<1	<1	<1	<1	<1	<1	<1
As	<5	<5	<5	<5	<5	<5	<5
B	11	<10	<10	<10	16	<10	<10
Ba	33	84.1	929	732	257	1210	710
Be	<5	<5	<5	6	<5	<5	<5
Bi	<0.1	0.1	<0.1	0.3	<0.1	<0.1	<0.1
Cd	<0.2	<0.2	<0.2	<0.2	<0.2	<0.2	<0.2
Ce	530	64.1	73.6	114	11.7	216	278
Co	1.7	0.8	0.6	3.8	0.6	3	3.3
Cr	24	30	33	44	22	19	34
Cs	0.3	1.2	0.6	0.4	0.9	2.1	1.3
Cu	<5	<5	<5	<5	<5	<5	7
Dy	4.33	3.69	4.43	4.64	2.39	4.71	5.22
Er	1.54	2.74	2.26	2.34	1.92	1.82	1.5
Eu	1.71	0.14	1.15	2.3	0.87	1.64	1.12
Ga	21.6	26	15.6	25	18.3	16.1	19.1
Gd	11.7	2.67	4.4	5.74	1.45	10.1	11.7
Ge	1	3	2	2	2	2	1
Hf	6	2	5	9	9	9	12
Ho	0.65	0.85	0.89	0.93	0.54	0.75	0.75
In	<0.2	<0.2	0.2	<0.2	<0.2	<0.2	<0.2
La	262	23.7	37.2	58	7.3	95.7	131
Li	<10	<10	<10	17	<10	12	12
Lu	0.23	0.6	0.31	0.44	0.39	0.2	0.21
Mn	63	161	51	192	239	139	115
Mo	3	3	3	3	2	<2	3
Nb	9.5	5.9	10.4	24.4	2.1	7.7	12.8
Nd	175	22	28.5	41.2	4.5	84	102
Ni	18	19	22	26	21	18	26
Pb	<5	22	21	9	33	38	56
Pr	55.8	7.21	8.9	12.4	1.42	23.9	30.7
Rb	21.6	171	223	72.5	302	309	258

Sample	MPAZ21-S6	MPAZ21-S7	MPAZ21-S8	MPAZ21-S2dup	D01	MPAZ21-S19	MRI20SD-38
Re	<0.02	<0.02	<0.02	<0.02	<0.02	<0.02	<0.02
Sb	0.1	<0.1	<0.1	<0.1	<0.1	0.2	<0.1
Sc	5	<5	9	9	<5	<5	<5
Se	<5	<5	<5	<5	<5	<5	<5
Sm	21.4	2.1	5	6.4	1.4	15	18.4
Sn	3	4	1	3	<1	1	3
Sr	21.8	30.2	246	270	65.4	169	133
Ta	0.6	0.6	<0.5	1.4	<0.5	<0.5	<0.5
Tb	1.32	0.49	0.71	0.87	0.31	1.18	1.3
Te	<0.5	<0.5	<0.5	<0.5	<0.5	<0.5	<0.5
Th	35.5	3.5	21.3	10.4	3.3	59.1	105
Tl	<0.5	1	1.1	<0.5	1.6	1.7	1.5
Tm	0.25	0.51	0.38	0.41	0.35	0.26	0.2
U	3.43	2.44	2	4.46	1.85	3.55	3.29
V	17	<5	25	45	<5	7	19
W	<1	<1	<1	<1	<1	<1	<1
Y	14.8	28.8	21	22.7	16.3	16.8	17.1
Yb	1.5	3.6	1.9	2.4	2.3	1.3	1.1
Zn	7	31	<5	7	<5	33	53
Zr	231	33.9	117	319	98.8	307	354

**Table 1. Whole-rock geochemical data from Lucy Gray Mountains and the McCullough Range (continued).**

Sample	MPMD21-S9	MPAZ21-S12	MPAZ21-S15	MPAZ21-S16	MPAZ21-S18	MPAZ21-S20	MPAZ21-S21
UnitName	Xmg	Xog	Xog	Xog	Xog	Xog	Xog
Quadrangle	McCullough	McCullough	Desert	Desert	Desert	Desert	Desert
Latitude	35.546591	35.53202	35.54423	35.54729	35.54201	35.539388	35.539375
Longitude	-115.215807	-115.17051	-115.297	-115.292705	-115.280622	-115.289467	-115.289601
Major elements (wt %)							
SiO <sub>2</sub>	73.7	70.1	71.4	71.5	71.4	63.8	66.7
TiO <sub>2</sub>	0.16	0.42	0.38	0.04	0.31	0.85	0.14
Al <sub>2</sub> O <sub>3</sub>	13.4	14.9	13.8	15.5	14.3	15.8	17
Fe <sub>2</sub> O <sub>3</sub>	2.55	3.23	3.22	0.34	2.83	6.86	1.58
MnO	0.02	0.04	0.04	<0.01	0.02	0.05	0.01
MgO	1.12	0.72	0.51	0.06	0.46	1.64	0.28
CaO	0.24	1.45	1.43	0.73	1.43	2.5	0.68
Na <sub>2</sub> O	5.76	3.13	2.36	2.61	2.49	4.51	3.01
K <sub>2</sub> O	0.59	4.45	5.72	8.5	6.25	1.54	9.06
P <sub>2</sub> O <sub>5</sub>	0.04	0.05	0.18	0.02	0.11	0.25	0.23
SrO	<0.01	<0.01	<0.01	<0.01	<0.01	0.02	0.03
BaO	<0.01	0.07	0.12	0.15	0.11	0.04	0.21
V <sub>2</sub> O <sub>5</sub>	<0.01	<0.01	<0.01	<0.01	<0.01	<0.01	<0.01
Cr <sub>2</sub> O <sub>3</sub>	<0.01	<0.01	<0.01	<0.01	<0.01	<0.01	<0.01
LOI*	1.17	1.25	0.77	0.36	0.64	1.93	0.86
Total	98.75	99.81	99.93	99.81	100.35	99.79	99.79
Minor and trace elements (ppm)							
Ag	<1	<1	<1	<1	<1	<1	<1
As	<5	<5	<5	<5	<5	<5	5
B	<10	<10	<10	<10	<10	<10	<10
Ba	71.9	632	916	1250	801	296	1400
Be	<5	<5	<5	<5	<5	<5	<5
Bi	<0.1	<0.1	<0.1	<0.1	<0.1	<0.1	<0.1
Cd	<0.2	<0.2	<0.2	<0.2	<0.2	<0.2	<0.2
Ce	85.9	75.4	195	12.1	226	104	464
Co	3	6	5.2	0.8	4.3	11.1	2
Cr	<10	29	18	13	25	31	18
Cs	0.1	1.3	1.3	0.9	1.1	0.5	1.3
Cu	<5	7	7	6	<5	5	7
Dy	10.4	4.37	5.07	0.82	4.27	9.21	12.7
Er	8.82	3.85	1.86	0.47	1.2	5.78	3.56
Eu	0.74	0.79	1.47	1.25	1.15	1.93	1.89
Ga	17.4	20.5	19.5	15.3	19.6	23.2	20.1
Gd	6.89	4.57	9.32	0.82	9.89	8.96	25.5
Ge	1	2	1	1	1	2	2
Hf	8	5	10	5	10	14	3
Ho	2.75	1.04	0.84	0.16	0.63	1.95	1.84
In	<0.2	<0.2	<0.2	<0.2	<0.2	<0.2	<0.2
La	39.7	37	95.3	6.3	105	49.2	220
Li	<10	11	18	<10	18	<10	<10
Lu	1.68	0.73	0.28	0.07	0.19	1.11	0.23
Mn	199	287	252	28	128	355	97
Mo	<2	<2	<2	<2	2	3	<2
Nb	6.1	22.7	18.7	1.6	12.3	16.1	6.4
Nd	37.2	27.1	74.4	4.3	84.5	46.9	179
Ni	14	22	15	17	26	23	16
Pb	<5	35	27	32	32	<5	58
Pr	10	8.06	21.2	1.35	24.5	12.3	53.3
Rb	28.6	188	247	279	228	91.5	276

Sample	MPMD21-S9	MPAZ21-S12	MPAZ21-S15	MPAZ21-S16	MPAZ21-S18	MPAZ21-S20	MPAZ21-S21
Re	<0.02	<0.02	<0.02	<0.02	<0.02	<0.02	<0.02
Sb	<0.1	<0.1	<0.1	<0.1	<0.1	<0.1	0.1
Sc	9	6	6	<5	5	16	<5
Se	6	<5	<5	<5	<5	<5	<5
Sm	7.9	5.9	13.5	0.9	14.1	10.2	31.7
Sn	<1	2	<1	<1	<1	8	1
Sr	54.3	153	112	137	85.7	232	211
Ta	<0.5	1.1	<0.5	<0.5	<0.5	1.3	<0.5
Tb	1.25	0.71	1.16	0.12	1.09	1.45	3.26
Te	<0.5	<0.5	<0.5	<0.5	<0.5	<0.5	<0.5
Th	22.5	18.7	44.4	4.8	72.8	19.8	164
Tl	<0.5	1.2	1.5	1.5	1.3	<0.5	1.5
Tm	1.55	0.6	0.25	0.1	0.16	0.91	0.41
U	2.11	2.37	2.97	2.75	4.26	3.57	3.91
V	8	33	13	<5	17	63	9
W	<1	<1	<1	<1	<1	<1	<1
Y	68.3	28.4	19	4.6	13.3	52.7	44.9
Yb	10	4.2	1.4	0.6	1.1	5.9	1.8
Zn	7	52	53	7	47	26	11
Zr	294	182	351	181	345	585	118

**Table 1. Whole-rock geochemical data from Lucy Gray Mountains and the McCullough Range (continued).**

Sample	MPAZ21-S23	MPAZ21-S24	MPAZ21-S25	MPAZ21-S27	MPAZ21-S28	MPAZ21-S16dup	D03
UnitName	Xog	Xog	Xog	Xog	Xog	Xog	Xog
Quadrangle	Desert	Desert	Desert	Desert	Desert	Desert	Desert
Latitude	35.582815	35.582493	35.582045	35.580786	35.587489	35.54729	35.584333
Longitude	-115.300059	-115.298054	-115.29253	-115.26123	-115.258091	-115.292705	-115.266037
Major elements (wt %)							
SiO <sub>2</sub>	77.7	74.8	74.2	72.4	72.9	72.6	72.8
TiO <sub>2</sub>	0.12	0.03	0.2	0.25	0.21	0.03	0.2
Al <sub>2</sub> O <sub>3</sub>	12	14	13	14.5	13.7	14.9	14
Fe <sub>2</sub> O <sub>3</sub>	1.16	0.33	1.53	2.34	1.86	0.3	1.84
MnO	0.01	<0.01	0.02	0.02	0.02	<0.01	0.02
MgO	0.15	0.07	0.18	0.45	0.28	0.06	0.3
CaO	0.57	1.01	0.99	1.22	1.04	0.69	1.22
Na <sub>2</sub> O	2.03	2.66	2.46	2.58	2.83	2.51	2.44
K <sub>2</sub> O	6.36	6.73	5.92	6.35	5.53	8.11	6.19
P <sub>2</sub> O <sub>5</sub>	0.01	0.15	0.03	0.06	0.03	0.02	0.04
SrO	<0.01	<0.01	<0.01	<0.01	<0.01	0.01	<0.01
BaO	0.06	0.1	0.1	0.09	0.06	0.14	0.07
V <sub>2</sub> O <sub>5</sub>	<0.01	<0.01	<0.01	<0.01	<0.01	<0.01	<0.01
Cr <sub>2</sub> O <sub>3</sub>	<0.01	<0.01	<0.01	<0.01	<0.01	<0.01	<0.01
LOI*	0.5	0.39	0.38	0.83	0.72	<0.01	0.63
Total	100.67	100.27	99.01	101.09	99.18	99.37	99.75
Minor and trace elements (ppm)							
Ag	<1	<1	<1	<1	<1	<1	<1
As	<5	<5	<5	<5	<5	<5	<5
B	<10	<10	<10	<10	<10	<10	<10
Ba	555	913	835	653	523	1190	556
Be	<5	<5	<5	<5	<5	<5	<5
Bi	<0.1	<0.1	<0.1	<0.1	<0.1	<0.1	<0.1
Cd	<0.2	<0.2	<0.2	<0.2	<0.2	<0.2	<0.2
Ce	84.6	17.3	122	199	133	11.7	109
Co	1.1	2.3	1.3	2.7	2.4	0.6	2.1
Cr	21	20	22	29	37	28	23
Cs	0.6	0.9	0.8	1.9	0.7	0.8	0.6
Cu	<5	6	<5	5	6	<5	5
Dy	2.46	3.03	4.12	19.6	15.7	0.64	2.45
Er	0.87	1.7	1.32	11.8	10.3	0.38	0.87
Eu	0.89	1.26	0.98	1.07	0.96	1.16	0.89
Ga	14.2	14.3	15.9	19.4	21	14.5	18.9
Gd	4.47	2.48	6.91	18.4	12.5	0.75	4.98
Ge	1	1	1	2	2	1	1
Hf	6	1	7	9	6	3	7
Ho	0.38	0.65	0.63	3.85	3.49	0.12	0.41
In	<0.2	<0.2	<0.2	<0.2	<0.2	<0.2	<0.2
La	41	6.6	59.8	94.1	61.1	6.3	48.4
Li	<10	<10	<10	13	<10	<10	<10
Lu	0.09	0.14	0.15	1.86	1.58	0.08	0.12
Mn	65	32	157	188	161	25	118
Mo	2	<2	3	3	3	2	2
Nb	6.4	1.4	6.1	20.1	20.4	1.3	8
Nd	34.5	5.9	49.1	85.1	55.5	4.5	41.9
Ni	20	17	21	22	31	24	34
Pb	30	27	25	50	45	30	31
Pr	9.59	1.67	13.9	24	15.1	1.24	11.8
Rb	203	242	223	269	268	271	203

Sample	MPAZ21-S23	MPAZ21-S24	MPAZ21-S25	MPAZ21-S27	MPAZ21-S28	MPAZ21-S16dup	D03
Re	<0.02	<0.02	<0.02	<0.02	<0.02	<0.02	<0.02
Sb	<0.1	<0.1	<0.1	1.2	<0.1	<0.1	<0.1
Sc	<5	<5	<5	7	<5	<5	<5
Se	<5	<5	<5	<5	<5	<5	<5
Sm	6.1	1.5	8.2	18.7	11.2	0.8	7.7
Sn	<1	<1	1	2	2	<1	<1
Sr	84.8	147	146	107	80.6	133	89.1
Ta	<0.5	<0.5	<0.5	1.1	0.7	<0.5	<0.5
Tb	0.54	0.45	0.91	3.02	2.26	0.1	0.57
Te	<0.5	<0.5	<0.5	<0.5	<0.5	<0.5	<0.5
Th	20.9	1.1	23.3	75.7	49.9	4.5	47.6
Tl	1.1	1.3	1.2	1.5	1.4	1.5	1
Tm	0.08	0.22	0.17	1.83	1.73	<0.05	0.12
U	2.3	1.11	2.85	9.13	6.92	1.71	3.09
V	<5	<5	6	11	10	<5	11
W	<1	<1	<1	<1	<1	<1	<1
Y	9.3	16.4	14.2	114	81.6	2.5	8.3
Yb	0.6	0.9	1	11.5	10.2	0.4	0.8
Zn	17	5	25	50	31	<5	21
Zr	150	37	204	249	205	140	216

**Table 1. Whole-rock geochemical data from Lucy Gray Mountains and the McCullough Range (continued).**

Sample	MPMD21-S8	MPAZ21-S22
UnitName	Xog	Xog
Quadrangle	McCullough	Desert
Latitude	35.552762	35.538746
Longitude	-115.205857	-115.28843

## Major elements (wt %)

SiO <sub>2</sub>	58.8	67.6
TiO <sub>2</sub>	0.76	0.08
Al <sub>2</sub> O <sub>3</sub>	18.7	17.6
Fe <sub>2</sub> O <sub>3</sub>	9.45	0.6
MnO	0.09	<0.01
MgO	2.77	0.19
CaO	0.68	0.51
Na <sub>2</sub> O	1.39	2.81
K <sub>2</sub> O	5.87	10.2
P <sub>2</sub> O <sub>5</sub>	0.06	0.16
SrO	<0.01	0.01
BaO	0.11	0.13
V <sub>2</sub> O <sub>5</sub>	0.02	<0.01
Cr <sub>2</sub> O <sub>3</sub>	0.02	<0.01
LOI*	0.93	0.56
Total	99.65	100.45

## Minor and trace elements (ppm)

Ag	<1	2
As	<5	<5
B	<10	<10
Ba	833	1110
Be	<5	<5
Bi	<0.1	<0.1
Cd	<0.2	<0.2
Ce	132	9.1
Co	22	1.4
Cr	102	<10
Cs	3.5	1.7
Cu	18	<5
Dy	7.72	1.8
Er	4.24	0.74
Eu	1.42	1.4
Ga	28	15.5
Gd	9.66	2.15
Ge	2	1
Hf	6	<1
Ho	1.62	0.35
In	<0.2	<0.2
La	66.6	5.2
Li	18	<10
Lu	0.57	0.06
Mn	646	62
Mo	<2	<2
Nb	19.8	3.6
Nd	56.9	4.4
Ni	52	7
Pb	33	45
Pr	15.9	1.39
Rb	255	301

Sample	MPMD21-S8	MPAZ21-S22
Re	<0.02	<0.02
Sb	<0.1	0.1
Sc	21	<5
Se	<5	<5
Sm	11.1	1.7
Sn	<1	<1
Sr	133	219
Ta	1.1	<0.5
Tb	1.47	0.34
Te	<0.5	<0.5
Th	24.8	1.8
Tl	1.4	1.6
Tm	0.59	0.09
U	2.71	0.26
V	114	<5
W	<1	<1
Y	41.4	8.7
Yb	3.7	0.5
Zn	135	11
Zr	190	4

\*LOI—loss on ignition

Analyses by AGAT Laboratories:

Inductively coupled plasma-optical emission spectrometry (ICP-OES) and inductively coupled plasma-mass spectrometry (ICP-MS) methods for minor and trace elements, and Wavelength Dispersive X-ray Fluorescence (WDXR) for major element oxides.

**Table 2. Summary compilation of new and published geochronologic data from the study area.**

Sample	Unit/ description	Latitude	Longitude	Phase	Method	Age (Ma)	$\pm 2\sigma$ (Ma)	n	MSWD	Reference	Notes
<i>Tertiary volcanic rocks</i>											
11-LG27	Tps / Peach Spring Tuff	35.57618	-115.25641	sanidine	$^{40}\text{Ar}/^{39}\text{Ar}$	<b>18.62</b>	<b>0.16</b>	11	1.6	This study	Weighted Mean
11-LG58	Tbs / tuff of Bridge Spring	35.56476	-115.24892	sanidine	$^{40}\text{Ar}/^{39}\text{Ar}$	<b>15.21</b>	<b>0.10</b>	12	1.3	This study	Weighted mean
0309LG4	Tdht / block-and-ash flow	35.59506	-115.24956	zircon	U-Pb	<b>17.99</b>	<b>0.26</b>	17	0.47	This study	Weighted mean
Fringe	Tbo / uppermost basalt flow	35.57421	-115.25382	zircon	U-Pb	<b>18.42</b>	<b>0.34</b>	12	0.75	This study	Weighted mean
<i>Proterozoic units</i>											
BBP1	Xbbp / Beer Bottle Pass pluton	35.62819	-115.27303	zircon	U-Pb	<b>1663</b>	<b>6</b>	31	0.9	This study	Weighted mean
BBP4	Xbbp / Beer Bottle Pass pluton	35.73587	-115.18277	zircon	U-Pb	<b>1658</b>	<b>6</b>	26	0.86	This study	Weighted mean
0204M1	McClanahan Spring pluton	35.68453	-115.16762	zircon	U-Pb	<b>1644</b>	<b>44</b>	34	43	This study	Discordia intercept
13		35.18036	-114.83185	zircon	U-Pb	<b>1685</b>	<b>8</b>	18	0.7	Almeida et al. (2016)	
17		35.22348	-114.78007	zircon	U-Pb	<b>1683.7</b>	<b>11.5</b>	17	0.4	Almeida et al. (2016)	
29		35.31128	-114.73550	zircon	U-Pb	<b>1681.1</b>	<b>11.9</b>	17	0.2	Almeida et al. (2016)	
35	Xbbp / Beer Bottle Pass pluton	35.6757	-115.29322	zircon	U-Pb	<b>1682.3</b>	<b>10.2</b>	17	0.64	Almeida et al. (2016)	
39 (1)	Xbbp / Beer Bottle Pass pluton	35.60387	-115.25973	zircon	U-Pb	<b>1681.6</b>	<b>7.9</b>	12	3.9	Almeida et al. (2016)	
39 (2)	Xbbp / Beer Bottle Pass pluton	35.60387	-115.25973	zircon	U-Pb	<b>1689.4</b>	<b>8.3</b>	27	1.12	Almeida et al. (2016)	
20		35.2049	-114.54813	zircon	U-Pb	<b>1683</b>	<b>4.7</b>	24	1.1	Almeida et al. (2016)	
22		35.21024	-114.59531	zircon	U-Pb	<b>1683.3</b>	<b>8.1</b>	18	0.6	Almeida et al. (2016)	
L		36.24232	-114.18947	zircon	U-Pb	<b>1372.5</b>	<b>42.1</b>	18	0.3	Almeida et al. (2016)	
W		36.21276	-114.14455	zircon	U-Pb	<b>1376.4</b>	<b>18.4</b>	12	0.25	Almeida et al. (2016)	
M84NY-82	Granite gneiss	35.37386	-115.24753	zircon	Pb-Pb	<b>1659</b>	<b>4</b>			Miller and Wooden (1994)	
M87NY-02	Xbt	35.4958	-115.15443	zircon	Pb-Pb	<b>1672</b>	<b>5</b>			Miller and Wooden (1994)	
M85NY-37	Xlgg	35.45793	-115.20903	zircon	Pb-Pb	<b>1674</b>	<b>10</b>			Miller and Wooden (1994)	
M84NY-06	Xmg	35.35485	-115.17633	zircon	Pb-Pb	<b>1683</b>	<b>22</b>			Miller and Wooden (1994)	
M88NY-07	Xmg	35.40775	-115.12018	zircon	Pb-Pb	<b>1683</b>	<b>22</b>			Miller and Wooden (1994)	
M88NY-28	Biotite granodiorite	35.44867	-115.12929	zircon	Pb-Pb	<b>1683</b>	<b>22</b>			Miller and Wooden (1994)	
JW88-108	Xmg	35.44867	-115.12929	zircon	Pb-Pb	<b>1683</b>	<b>22</b>			Miller and Wooden (1994)	
M87NY-01	Xlg?	35.50483	-115.12700	zircon	Pb-Pb	<b>1686</b>	<b>12</b>			Miller and Wooden (1994)	
M84NY-77	Xag	35.35604	-115.23405	zircon	Pb-Pb	<b>1708</b>	<b>12</b>			Miller and Wooden (1994)	
MPAZ21-S14	Xgr	35.52981	-115.16921	zircon	U-Pb	<b>1642</b>	<b>13</b>	7	0.6	Zuza et al. (2022)	Weighted Mean
MPAZ21-S29	Xg	35.56019	-115.14065	zircon	U-Pb	<b>1641</b>	<b>34</b>	17	11.5	Zuza et al. (2022)	Discordia intercept
MPAZ21-S26	Xog	35.58151	-115.28339	zircon	U-Pb	<b>1660</b>	<b>15</b>	5	1	This study	Weighted Mean
MPAZ21-S7	Xog	35.52807	-115.14045	zircon	U-Pb	<b>1672</b>	<b>64</b>	14	5.2	Zuza et al. (2022)	Discordia intercept
MPAZ21-S17	Xog	35.5474	-115.29257	zircon	U-Pb	<b>1622</b>	<b>24</b>	11	3	This study	Weighted Mean
MRI20SD-19	Xbkg	35.49128	-115.16073	zircon	U-Pb	<b>1658</b>	<b>13</b>	23	2.3	Zuza et al. (2022)	Weighted Mean
MPAZ21-S3	Xbkg	35.52544	-115.15304	zircon	U-Pb	<b>1657</b>	<b>8</b>	38	1.5	Zuza et al. (2022)	Weighted mean
MPAZ21-S34	Xbkg	35.50379	-115.18382	zircon	U-Pb	<b>1667</b>	<b>13</b>	34	2.8	Zuza et al. (2022)	Weighted mean

Sample	Unit/ description	Latitude	Longitude	Phase	Method	Age (Ma)	$\pm 2\sigma$ (Ma)	n	MSWD	Reference	Notes
IV1		35.44295	-115.41392	zircon	Pb-Pb	<b>1764</b>	<b>12</b>		1.6	Strickland et al. (2013)	
IV5		35.44295	-115.41392	zircon	Pb-Pb	<b>1759</b>	<b>8</b>		0.88	Strickland et al. (2013)	
IV21		35.42952	-115.43082	zircon	Pb-Pb	<b>1744</b>	<b>10</b>		0.94	Strickland et al. (2013)	
IV40		35.40715	-115.43338	zircon	Pb-Pb	<b>1737</b>	<b>18</b>		22	Strickland et al. (2013)	
IV45		35.41633	-115.43427	zircon	Pb-Pb	<b>1663</b>	<b>6</b>		1.2	Strickland et al. (2013)	
IV95		35.40428	-115.43367	zircon	Pb-Pb	<b>1730</b>	<b>25</b>		19	Strickland et al. (2013)	
IV96		35.40432	-115.43383	zircon	Pb-Pb	<b>1661</b>	<b>9</b>		2.3	Strickland et al. (2013)	
IV22		35.42948	-115.42787	meta. zircon	Pb-Pb	<b>1760</b>	<b>18</b>		1.6	Strickland et al. (2013)	
IV41		35.40715	-115.43338	meta. zircon	Pb-Pb	<b>1716</b>				Strickland et al. (2013)	
IV46		35.41633	-115.43427	meta. zircon	Pb-Pb	<b>1702</b>	<b>7</b>		0.77	Strickland et al. (2013)	
IV63		35.42312	-115.41465	meta. zircon	Pb-Pb	<b>1706</b>				Strickland et al. (2013)	
IV65		35.42473	-115.42410	meta. zircon	Pb-Pb	<b>1661</b>	<b>12</b>		0.45	Strickland et al. (2013)	
IV67		35.42455	-115.42537	meta. zircon	Pb-Pb	<b>1738</b>	<b>20</b>		3.9	Strickland et al. (2013)	

**Table 3.**  $^{40}\text{Ar}/^{39}\text{Ar}$  geochronology results from this study.

11-LG27, Single Crystal Sanidine, $J = 0.001711 \pm 0.32\%$												
Peach Spring Tuff (Tps; 35.57618, -115.25641)												
4 amu discrimination = $1.0614 \pm 0.56\%$ , $40/39\text{K} = 0.0243 \pm 80.90\%$ , $36/37\text{Ca} = 0.000239 \pm 8.17\%$ , $39/37\text{Ca} = 0.000655 \pm 3.50\%$												
Crystal	T (C)	t (min.)	$^{36}\text{Ar}$	$^{37}\text{Ar}$	$^{38}\text{Ar}$	$^{39}\text{Ar}$	$^{40}\text{Ar}$	% $^{40}\text{Ar}^*$	Ca/K	$^{40}\text{Ar}^*/^{39}\text{ArK}$	Age (Ma)	1s.d.
1	1600	2	0.115	0.038	0.736	54.361	360.704	92.9	0.075783271	6.1862	<b>19.00</b>	<b>0.17</b>
2	1600	2	0.081	0.037	0.402	29.243	11-	92.0	0.137171362	6.0124	<b>18.46</b>	<b>0.18</b>
3	1600	2	0.371	0.049	0.675	46.072	378.431	74.3	0.115302935	6.1266	<b>18.81</b>	<b>0.21</b>
4	1600	2	0.166	0.057	0.475	33.786	242.933	83.8	0.182905409	6.0114	<b>18.46</b>	<b>0.18</b>
5	1600	2	0.387	0.052	0.822	56.526	444.602	77.1	0.099732062	6.0955	<b>18.72</b>	<b>0.21</b>
6	1600	2	0.171	0.057	0.758	53.970	359.372	88.5	0.114499529	5.9135	<b>18.16</b>	<b>0.19</b>
7	1600	2	0.337	0.048	0.612	41.118	336.422	73.9	0.126558637	6.0644	<b>18.62</b>	<b>0.24</b>
8	1600	2	0.298	0.039	0.619	42.187	335.506	77.1	0.100222614	6.1482	<b>18.88</b>	<b>0.19</b>
9	1600	2	0.178	0.046	0.681	48.856	338.429	87.3	0.102075115	6.0598	<b>18.61</b>	<b>0.21</b>
10	1600	2	0.960	0.055	0.945	58.579	611.079	57.1	0.101788956	5.9993	<b>18.42</b>	<b>0.24</b>
11	1600	2	0.095	0.053	0.825	61.796	392.486	94.9	0.092981062	6.0516	<b>18.58</b>	<b>0.16</b>
12	1600	2	0.210	0.049	0.714	51.282	344.366	84.9	0.103588427	5.7133	<b>17.55</b>	<b>0.17</b>
note: isotope beams in mV rlsd = released, error in age includes J error, all errors 1 sigma												
(36Ar through 40Ar are measured beam intensities, corrected for decay in age calculations)												
11-LG58, Single Crystal Sanidine, $J = 0.001706 \pm 0.44\%$												
tuff of Bridge Spring (Tbs; 35.56476, -115.24892)												
4 amu discrimination = $1.0527 \pm 0.41\%$ , $40/39\text{K} = 0.0243 \pm 80.90\%$ , $36/37\text{Ca} = 0.000239 \pm 8.17\%$ , $39/37\text{Ca} = 0.000655 \pm 3.50\%$												
Crystal	T (C)	t (min.)	$^{36}\text{Ar}$	$^{37}\text{Ar}$	$^{38}\text{Ar}$	$^{39}\text{Ar}$	$^{40}\text{Ar}$	% $^{40}\text{Ar}^*$	Ca/K	$^{40}\text{Ar}^*/^{39}\text{ArK}$	Age (Ma)	1s.d.
1	1600	2	0.200	0.092	1.352	98.213	536.426	90.4	0.106092727	4.9658	<b>15.22</b>	<b>0.13</b>
2	1600	2	0.308	0.075	0.820	55.084	352.787	77.0	0.154208255	4.9438	<b>15.15</b>	<b>0.13</b>
3	1600	2	0.228	0.062	0.816	56.891	346.987	83.1	0.123428858	5.0814	<b>15.57</b>	<b>0.13</b>
4	1600	2	0.433	0.071	0.992	66.260	445.424	73.8	0.121359921	4.9844	<b>15.28</b>	<b>0.14</b>
5	1600	2	0.433	0.008	1.151	78.871	507.519	77.0	0.011487603	4.9802	<b>15.26</b>	<b>0.13</b>
6	1600	2	0.283	0.089	1.328	98.136	600.131	87.5	0.102713626	5.3863	<b>16.50</b>	<b>0.16</b>
7	1600	2	0.237	0.119	0.728	51.309	312.077	80.4	0.262685844	4.9025	<b>15.03</b>	<b>0.16</b>
8	1600	2	0.595	0.101	1.456	98.858	653.492	75.1	0.115711714	4.9972	<b>15.32</b>	<b>0.15</b>
9	1600	2	0.681	0.124	0.907	57.288	453.332	58.9	0.245154255	4.6824	<b>14.35</b>	<b>0.19</b>
10	1600	2	0.900	0.258	1.244	81.640	667.857	62.9	0.35793981	5.1798	<b>15.87</b>	<b>0.18</b>
11	1600	2	0.283	0.078	0.761	52.104	328.578	77.4	0.169549684	4.8947	<b>15.00</b>	<b>0.13</b>
12	1600	2	0.346	0.065	0.706	46.477	319.540	71.2	0.158397215	4.9078	<b>15.04</b>	<b>0.14</b>

Crystal	T (C)	t (min.)	<sup>36</sup> Ar	<sup>37</sup> Ar	<sup>38</sup> Ar	<sup>39</sup> Ar	<sup>40</sup> Ar	% <sup>40</sup> Ar*	Ca/K	<sup>40</sup> Ar*/ <sup>39</sup> ArK	Age (Ma)	1s.d.	
13	1600	2	0.118	0.077	1.042	77.360	411.429	93.2	0.112730576	4.9772	<b>15.25</b>	<b>0.12</b>	
14	1600	2	0.342	0.084	1.056	74.052	456.331	80.0	0.128472925	4.9556	<b>15.19</b>	<b>0.13</b>	
15	1600	2	0.217	0.088	1.202	87.214	486.302	88.5	0.114278384	4.9585	<b>15.20</b>	<b>0.13</b>	
note: isotope beams in mV rlsd = released, error in age includes J error, all errors 1 sigma											Mean ± s.d. =	15.28	0.45
( <sup>36</sup> Ar through <sup>40</sup> Ar are measured beam intensities, corrected for decay in age calculations)											<b>Wtd mean age =</b>	<b>15.21</b>	<b>0.05</b>
(12 fusions)													
No isochron													

**Table 4. U-Pb zircon geochronology results from this study.**

Analysis	U	206Pb	Th/U	206Pb*	±	207Pb*	±	206Pb*	±	error	206Pb*	±	207Pb*	±	206Pb*	±	Best age	±	Conc	Ex
	(ppm)	204Pb		207Pb*	(%)	235U	(%)	238U	(%)	corr.	238U	(Ma)	235U	(Ma)	207Pb*	(Ma)	(Ma)	(Ma)	(%)	*
<b>MPAZ21-S26 (Xog, 35.58151, -115.283391)</b>																				
MPAZ21-S26 - 1	2615.2	47689.2	0.04	10.29	1.36	3.25	1.72	0.24	1.06	0.62	1411.6	13.5	1468.7	13.4	1552.4	25.5	1552.4	25.5	90.9	x
MPAZ21-S26 - 10	3504.7	219889.3	0.04	10.34	1.02	3.36	1.41	0.25	0.98	0.69	1437.3	12.6	1495.5	11.1	1579.0	19.1	1579.0	19.1	91.0	x
MPAZ21-S26 - 11	1866.9	307252.7	0.04	9.99	0.92	4.08	1.36	0.29	1.00	0.73	1662.1	14.6	1650.8	11.1	1636.6	17.2	1636.6	17.2	101.6	x
MPAZ21-S26 - 13	3251.7	186870.8	0.04	10.12	1.01	3.96	1.54	0.29	1.17	0.76	1637.1	16.9	1626.2	12.5	1612.2	18.8	1612.2	18.8	101.5	x
MPAZ21-S26 - 15	2878.1	69891.0	0.07	9.82	0.88	4.36	1.51	0.31	1.22	0.81	1739.3	18.7	1705.6	12.5	1664.4	16.3	1664.4	16.3	104.5	
MPAZ21-S26 - 17	1731.2	149667.1	0.08	10.12	1.22	3.67	2.44	0.27	2.12	0.87	1532.7	28.9	1564.7	19.5	1608.1	22.8	1608.1	22.8	95.3	x
MPAZ21-S26 - 19	3209.3	172069.0	0.05	10.38	0.84	3.13	1.52	0.23	1.27	0.83	1357.1	15.5	1438.9	11.7	1561.9	15.8	1561.9	15.8	86.9	x
MPAZ21-S26 - 2	149.2	5246.4	0.83	9.17	2.17	4.17	3.99	0.28	3.26	0.82	1613.3	46.5	1668.4	32.7	1738.5	42.3	1738.5	42.3	92.8	x
MPAZ21-S26 - 20	2247.6	33646.1	0.06	9.99	0.94	3.73	1.38	0.27	1.00	0.73	1542.2	13.8	1578.4	11.0	1627.1	17.6	1627.1	17.6	94.8	x
MPAZ21-S26 - 22	3046.3	266578.4	0.03	10.19	0.94	3.66	1.81	0.27	1.55	0.86	1537.1	21.2	1562.4	14.5	1596.7	17.5	1596.7	17.5	96.3	x
MPAZ21-S26 - 23	690.6	43240.9	0.25	9.91	1.26	4.23	1.96	0.30	1.50	0.76	1707.3	22.5	1679.0	16.1	1643.8	23.5	1643.8	23.5	103.9	
MPAZ21-S26 - 27	1760.1	67972.1	0.07	10.17	1.00	3.10	1.81	0.23	1.51	0.83	1323.3	18.1	1432.0	13.9	1597.4	18.6	1597.4	18.6	82.8	x
MPAZ21-S26 - 29	2991.8	117166.4	0.04	9.87	0.80	3.99	1.24	0.28	0.95	0.77	1615.7	13.5	1632.4	10.0	1654.0	14.7	1654.0	14.7	97.7	
MPAZ21-S26 - 3	2787.3	30311.3	0.04	10.13	1.07	3.21	1.63	0.24	1.23	0.75	1370.1	15.2	1458.7	12.6	1590.2	20.0	1590.2	20.0	86.2	x
MPAZ21-S26 - 30	2985.3	130395.6	0.05	9.98	0.94	3.86	1.63	0.28	1.34	0.82	1584.8	18.8	1605.9	13.2	1633.6	17.4	1633.6	17.4	97.0	x
MPAZ21-S26 - 31	3354.2	6632.7	0.05	9.49	0.95	3.57	1.37	0.25	0.99	0.72	1427.9	12.6	1542.5	10.9	1703.4	17.5	1703.4	17.5	83.8	x
MPAZ21-S26 - 32	3029.9	195543.3	0.04	10.44	1.05	2.88	1.61	0.22	1.23	0.76	1260.9	14.0	1376.5	12.2	1560.6	19.7	1560.6	19.7	80.8	x
MPAZ21-S26 - 33	3956.2	34058.5	0.07	10.63	0.81	3.13	1.10	0.24	0.74	0.67	1385.4	9.3	1439.6	8.5	1520.7	15.3	1520.7	15.3	91.1	x
MPAZ21-S26 - 34	4019.9	59755.5	0.06	10.00	0.92	3.46	1.27	0.25	0.87	0.69	1439.8	11.3	1517.1	10.0	1626.7	17.1	1626.7	17.1	88.5	x
MPAZ21-S26 - 35	2539.4	66233.8	0.06	9.88	0.87	3.66	1.53	0.26	1.26	0.82	1501.3	16.9	1563.3	12.2	1648.1	16.2	1648.1	16.2	91.1	x
MPAZ21-S26 - 36	3469.8	285361.3	0.05	10.24	0.86	3.18	1.41	0.23	1.13	0.80	1360.0	13.8	1452.6	10.9	1590.8	16.0	1590.8	16.0	85.5	x
MPAZ21-S26 - 38	2924.0	139604.0	0.04	10.28	1.02	3.68	1.59	0.27	1.22	0.77	1555.9	16.9	1567.8	12.7	1583.8	19.1	1583.8	19.1	98.2	x
MPAZ21-S26 - 39	2261.6	153213.6	0.04	10.27	0.84	3.56	1.24	0.27	0.91	0.73	1517.9	12.3	1540.1	9.8	1570.8	15.8	1570.8	15.8	96.6	x
MPAZ21-S26 - 40	2426.4	179990.4	0.03	9.88	0.80	4.25	1.40	0.30	1.15	0.82	1708.6	17.2	1684.5	11.5	1654.6	14.8	1654.6	14.8	103.3	
MPAZ21-S26 - 41	2700.9	185131.9	0.04	10.15	0.94	3.69	1.63	0.27	1.33	0.82	1545.2	18.3	1568.2	13.0	1599.3	17.5	1599.3	17.5	96.6	x
MPAZ21-S26 - 43	2524.0	158867.4	0.04	10.36	1.00	3.10	1.90	0.23	1.62	0.85	1352.2	19.7	1432.4	14.6	1553.7	18.8	1553.7	18.8	87.0	x
MPAZ21-S26 - 45	2771.8	69576.5	0.05	9.51	1.53	4.30	2.15	0.30	1.52	0.70	1678.2	22.4	1692.8	17.7	1711.0	28.1	1711.0	28.1	98.1	
MPAZ21-S26 - 46	3206.8	34650.8	0.05	9.89	0.90	3.89	1.55	0.28	1.27	0.82	1601.2	18.0	1610.7	12.6	1623.2	16.7	1623.2	16.7	98.6	x
MPAZ21-S26 - 47	1931.3	34256.9	0.03	10.18	0.93	3.22	1.66	0.24	1.37	0.83	1397.2	17.2	1460.8	12.8	1554.5	17.5	1554.5	17.5	89.9	x
MPAZ21-S26 - 50	2882.7	149816.1	0.04	10.38	0.83	3.04	1.66	0.23	1.44	0.87	1348.4	17.5	1418.1	12.7	1524.2	15.7	1524.2	15.7	88.5	x
MPAZ21-S26 - 6	3161.5	183636.2	0.03	9.97	0.99	3.94	1.39	0.29	0.97	0.70	1617.9	13.8	1622.7	11.2	1628.8	18.5	1628.8	18.5	99.3	x
MPAZ21-S26 - 7	2613.4	137289.0	0.03	10.16	1.02	3.30	1.55	0.24	1.17	0.75	1392.8	14.6	1481.4	12.1	1610.7	19.1	1610.7	19.1	86.5	x
MPAZ21-S26 - 8	2712.1	390263.2	0.05	9.86	1.09	3.74	1.70	0.27	1.31	0.77	1516.4	17.7	1580.6	13.6	1667.2	20.1	1667.2	20.1	91.0	x
MPAZ21-S26 - 9	1729.1	179506.9	0.02	10.24	0.95	3.88	1.68	0.29	1.39	0.83	1620.2	19.8	1609.9	13.5	1596.4	17.7	1596.4	17.7	101.5	x
<b>MPAZ21-S17 (Xog, 35.5474, -115.292568)</b>																				
MPAZ21-S17 - 3	1525.1	35324.0	0.24	10.04	0.86	3.68	1.32	0.27	0.99	0.75	1558.7	13.7	1568.1	10.5	1580.7	16.2	1580.7	16.2	98.6	
MPAZ21-S17 - 12	310.8	95977.0	0.48	10.04	2.24	3.80	3.95	0.28	3.25	0.82	1611.8	46.3	1593.0	31.7	1568.1	42.1	1568.1	42.1	102.8	
MPAZ21-S17 - 15	2188.5	271549.1	0.37	9.87	0.91	3.89	2.38	0.28	2.20	0.92	1611.3	31.3	1612.2	19.2	1613.4	16.9	1613.4	16.9	99.9	
MPAZ21-S17 - 29	316.6	76565.3	1.30	9.62	2.29	4.23	4.23	0.30	3.56	0.84	1694.1	53.0	1679.2	34.7	1660.7	42.4	1660.7	42.4	102.0	
MPAZ21-S17 - 34	3553.9	43584.3	0.03	9.45	0.82	4.47	1.56	0.31	1.32	0.85	1762.7	20.4	1725.6	12.9	1681.0	15.2	1681.0	15.2	104.9	
MPAZ21-S17 - 37	547.4	10460.6	1.19	9.64	1.03	3.72	2.14	0.27	1.80	0.84	1537.7	24.7	1575.7	17.1	1627.0	21.5	1627.0	21.5	94.5	
MPAZ21-S17 - 40	450.6	200184.2	1.21	9.91	1.74	3.99	2.89	0.29	2.31	0.80	1652.7	33.7	1632.7	23.5	1607.0	32.5	1607.0	32.5	102.8	
MPAZ21-S17 - 41	816.9	7673.7	0.08	9.49	1.41	4.26	1.97	0.30	1.34	0.68	1710.5	20.2	1685.4	16.2	1654.3	26.7	1654.3	26.7	103.4	
MPAZ21-S17 - 45	892.0	122119.4	1.17	10.04	1.02	3.93	1.86	0.29	1.56	0.84	1646.4	22.7	1620.4	15.1	1586.7	19.0	1586.7	19.0	103.8	
MPAZ21-S17 - 46	335.3	91693.4	1.02	9.73	1.65	4.08	3.50	0.29	3.09	0.88	1658.1	45.2	1649.9	28.6	1639.5	30.6	1639.5	30.6	101.1	
MPAZ21-S17 - 47	846.4	87961.1	1.17	9.85	0.74	4.11	1.64	0.30	1.46	0.89	1690.0	21.8	1657.1	13.4	1615.7	13.8	1615.7	13.8	104.6	

Analysis	U	206Pb	Th/U	206Pb*	±	207Pb*	±	206Pb*	±	error	206Pb*	±	207Pb*	±	206Pb*	±	Best age	±	Conc	Ex
																			*	
<b>0309LG4 (Tdht, 35.56506, -115.24956)</b>																				
0309LG4 Spot 1	245	11570	0.7	22.0261	3.2	0.0177	4.4	0.0028	3.1	0.70	18.2	0.6	17.8	0.8	34.1	76.8	18.19	0.56	NA	
0309LG4 Spot 2	271	594	0.5	38.0205	4.3	0.0099	5.2	0.0027	3.0	0.57	17.6	0.5	10.0	0.5	1583.2	146.0	17.64	0.52	NA	
0309LG4 Spot 3	198	973	0.5	21.7642	10.4	0.0174	10.7	0.0028	2.5	0.24	17.7	0.4	17.5	1.9	5.1	251.7	17.70	0.45	NA	
0309LG4 Spot 4	206	570	0.8	54.1702	11.7	0.0070	12.3	0.0027	3.9	0.32	17.7	0.7	7.1	0.9	3004.0	1223	17.65	0.70	NA	
0309LG4 Spot 5	211	750	0.4	32.5024	19.5	0.0116	19.7	0.0027	3.3	0.16	17.6	0.6	11.7	2.3	1082.0	591.9	17.61	0.57	NA	
0309LG4 Spot 6	323	1534	0.3	25.2360	9.5	0.0153	10.0	0.0028	3.0	0.30	18.0	0.5	15.4	1.5	375.3	247.5	17.98	0.54	NA	
0309LG4 Spot 7	242	4255	0.3	20.6624	5.0	0.0187	5.4	0.0028	2.1	0.39	18.1	0.4	18.8	1.0	118.7	117.0	18.06	0.38	NA	
0309LG4 Spot 8	204	19120	0.8	19.3305	4.2	0.0198	5.2	0.0028	3.1	0.59	17.9	0.6	19.9	1.0	273.6	96.1	17.88	0.55	NA	
0309LG4 Spot 9	301	1697	1.0	23.3736	10.9	0.0169	11.2	0.0029	2.7	0.24	18.4	0.5	17.0	1.9	180.2	272.9	18.45	0.50	NA	
10309LG4 Spot 0	586	59970	0.9	21.3013	2.4	0.0177	3.7	0.0027	2.8	0.76	17.6	0.5	17.8	0.7	46.5	57.9	17.62	0.50	NA	
0309LG4 Spot 11	239	12646	0.6	20.6082	3.1	0.0190	4.0	0.0028	2.5	0.62	18.2	0.5	19.1	0.8	124.9	73.8	18.23	0.46	NA	
0309LG4 Spot 12	202	1525	0.8	23.1848	8.2	0.0165	8.8	0.0028	3.1	0.36	17.9	0.6	16.6	1.5	160.0	205.4	17.88	0.56	NA	
0309LG4 Spot 13	514	1499	0.8	24.5595	6.0	0.0159	6.6	0.0028	2.6	0.39	18.2	0.5	16.0	1.0	305.2	154.5	18.19	0.46	NA	
0309LG4 Spot 14	330	676	0.4	38.5408	21.0	0.0097	21.2	0.0027	2.6	0.12	17.5	0.5	9.9	2.1	1629.5	726.7	17.54	0.46	NA	
0309LG4 Spot 15	182	374	0.6	109.512	64.2	0.0035	64.3	0.0027	2.7	0.04	17.7	0.5	3.5	2.2	0.0	842.0	17.66	0.48	NA	
0309LG4 Spot 16	110	4245	2.1	19.8891	5.0	0.0193	6.8	0.0028	4.5	0.67	17.9	0.8	19.4	1.3	207.9	116.8	17.91	0.81	NA	
0309LG4 Spot 17	639	5325	0.3	19.9372	2.0	0.0193	2.9	0.0028	2.1	0.73	18.0	0.4	19.5	0.6	202.3	46.0	18.01	0.38	NA	
0309LG4 Spot 20	302	573	0.7	42.6890	6.4	0.0085	7.1	0.0026	3.0	0.42	17.0	0.5	8.6	0.6	1995.5	240.3	16.98	0.51	NA	
0309LG4 Spot 21	199	1252	0.9	26.3307	12.9	0.0145	14.0	0.0028	5.4	0.38	17.8	1.0	14.6	2.0	486.7	344.8	17.77	0.95	NA	
0309LG4 Spot 22	163	264	1.1	-54.63	4.1	-0.0070	5.6	0.0028	3.9	0.69	17.9	0.7	7.1	0.4	0.0	0.0	17.85	0.69	NA	
0309LG4 Spot 23	147	833	0.3	27.8895	5.9	0.0138	6.7	0.0028	3.2	0.47	18.0	0.6	14.0	0.9	641.9	162.8	18.03	0.57	NA	
0309LG4 Spot 24	260	2360	0.8	23.5168	3.4	0.0164	4.4	0.0028	2.9	0.64	18.0	0.5	16.5	0.7	195.5	85.1	17.99	0.51	NA	
0309LG4 Spot 25	137	261	0.6	-264.15	104.5	-0.0013	104.6	0.0026	3.9	0.04	16.5	0.6	1.4	1.4	0.0	644.6	16.49	0.64	NA	
0309LG4 Spot 26	64	2898	1.5	18.8195	7.3	0.0207	8.3	0.0028	3.9	0.47	18.2	0.7	20.9	1.7	334.6	166.3	18.23	0.71	NA	
0309LG4 Spot 27	238	397	0.9	131.84	71.8	0.0028	71.9	0.0026	3.2	0.04	17.0	0.5	2.8	2.0	0.0	753.1	17.01	0.54	NA	
0309LG4 Spot 28	300	520	0.8	35.1980	11.8	0.0108	12.1	0.0028	2.4	0.20	17.8	0.4	10.9	1.3	1329.4	379.5	17.80	0.43	NA	
0309LG4 Spot 29	123	959	1.1	29.6850	4.3	0.0134	5.9	0.0029	4.1	0.69	18.5	0.8	13.5	0.8	816.2	121.2	18.53	0.75	NA	
0309LG4 Spot 30	180	481	0.4	55.4207	16.0	0.0067	16.3	0.0027	2.9	0.18	17.4	0.5	6.8	1.1	3115.6	1166	17.38	0.51	NA	
0309LG4 Spot 31	268	625	0.9	41.5073	13.7	0.0090	14.0	0.0027	3.1	0.22	17.4	0.5	9.1	1.3	1891.7	501.7	17.40	0.54	NA	
0309LG4 Spot 32	221	611	0.4	45.5861	24.5	0.0117	24.9	0.0039	4.7	0.19	24.9	1.2	11.8	2.9	2249.1	988.2	24.92	1.16	NA	
0309LG4 Spot 33	277	7559	0.7	20.5749	2.6	0.0191	3.6	0.0029	2.4	0.68	18.4	0.4	19.2	0.7	128.7	62.2	18.37	0.45	NA	
0309LG4 Spot 34	329	1046	1.1	30.3700	6.6	0.0124	7.4	0.0027	3.4	0.46	17.5	0.6	12.5	0.9	881.6	191.4	17.54	0.59	NA	
0309LG4 Spot 35	310	1280	1.1	23.2174	2.5	0.0165	4.0	0.0028	3.1	0.78	17.9	0.6	16.6	0.7	163.5	61.5	17.89	0.55	NA	
<b>Fringe (Tbo, 35.57421, -115.25382)</b>																				
Fringe Spot 1	437	9830	0.4	23.0142	2.8	0.0174	4.1	0.0029	3.0	0.73	18.7	0.6	17.6	0.7	NA	NA	18.74	0.56	NA	
Fringe Spot 2	1058	20670	0.2	20.5373	2.2	0.0193	3.5	0.0029	2.7	0.78	18.5	0.5	19.4	0.7	133.0	50.8	18.48	0.50	NA	
Fringe Spot 3	312	3914	0.7	24.3730	5.2	0.0165	6.1	0.0029	3.2	0.53	18.8	0.6	16.6	1.0	NA	NA	18.80	0.61	NA	
Fringe Spot 5	581	107177	0.2	21.2240	2.4	0.0218	4.9	0.0033	4.2	0.86	21.6	0.9	21.8	1.0	55.1	58.1	21.56	0.90	NA	
Fringe Spot 6	896	33516	0.4	21.5885	2.0	0.0179	3.8	0.0028	3.2	0.85	18.1	0.6	18.0	0.7	14.4	48.1	18.07	0.58	NA	
Fringe Spot 7	615	16973	0.3	21.8024	2.2	0.0188	4.3	0.0030	3.7	0.86	19.2	0.7	18.9	0.8	NA	NA	19.16	0.70	NA	
Fringe Spot 8	1161	66657	0.3	18.9622	2.8	0.0212	4.0	0.0029	2.8	0.71	18.7	0.5	21.3	0.8	317.5	64.7	18.73	0.53	NA	
Fringe Spot 9	75	15717	0.7	22.4028	3.2	0.0683	4.5	0.0111	3.1	0.69	71.2	2.2	67.1	2.9	NA	NA	71.22	2.19	NA	
Fringe Spot 10	56	24450	1.8	22.3133	3.4	0.0679	4.2	0.0110	2.5	0.59	70.5	1.7	66.7	2.7	NA	NA	70.46	1.73	NA	
Fringe Spot 11	1177	1165912	0.0	9.9148	1.3	4.1372	3.4	0.2976	3.2	0.92	1679.5	47.1	1661.7	28.2	1640.0	24.4	1639.96	24.37	102.4	
Fringe Spot 12	260	17113	0.9	21.3704	1.7	0.0742	3.6	0.0115	3.1	0.87	73.8	2.3	72.7	2.5	38.7	41.7	73.76	2.28	NA	
Fringe Spot 13	470	66358528	0.4	9.5684	1.4	3.3966	3.5	0.2358	3.2	0.92	1364.9	40.0	1503.6	27.7	1705.7	25.2	1705.70	25.18	80.0	
Fringe Spot 14	637	1074820	0.1	9.4211	1.1	3.8578	3.8	0.2637	3.6	0.95	1508.8	48.6	1604.9	30.5	1734.2	20.7	1734.22	20.67	87.0	
Fringe Spot 15	613	115690	0.3	21.1890	2.1	0.0182	4.0	0.0028	3.4	0.85	18.0	0.6	18.3	0.7	59.1	50.5	18.03	0.62	NA	
Fringe Spot 18	333	75513	0.9	22.0756	2.8	0.0180	5.2	0.0029	4.4	0.84	18.6	0.8	18.1	0.9	NA	NA	18.58	0.82	NA	

Analysis	U	206Pb	Th/U	206Pb*	$\pm$	207Pb*	$\pm$	206Pb*	$\pm$	error	206Pb*	$\pm$	207Pb*	$\pm$	206Pb*	$\pm$	Best age	$\pm$	Conc	Ex *
Fringe Spot 19	2291	185918	0.1	22.0623	1.5	0.0178	3.3	0.0028	3.0	0.90	18.3	0.5	17.9	0.6	NA	NA	18.31	0.55	NA	
Fringe Spot 21	779	27003	0.3	20.6915	2.8	0.0194	4.4	0.0029	3.3	0.76	18.8	0.6	19.6	0.8	115.4	66.2	18.80	0.63	NA	
Fringe Spot 22	1956	2410224	0.3	21.2653	1.9	0.0178	4.0	0.0027	3.5	0.88	17.7	0.6	17.9	0.7	50.5	45.6	17.66	0.61	NA	
Fringe Spot 23	449	89826	1.0	20.8985	2.5	0.0192	4.4	0.0029	3.6	0.83	18.8	0.7	19.4	0.8	91.9	58.3	18.79	0.68	NA	
Fringe Spot 24	1019	6420380	0.1	9.8948	1.3	3.9842	3.4	0.2860	3.1	0.92	1621.8	44.4	1631.0	27.4	1643.7	24.8	1643.71	24.84	98.7	x
Fringe Spot 25	857	2128940	0.3	9.7731	1.3	3.9666	3.8	0.2813	3.6	0.94	1597.8	50.5	1627.4	30.9	1666.6	25.0	1666.63	24.97	95.9	x
Fringe Spot 26	311	124706	0.4	17.6738	3.0	0.0228	4.6	0.0029	3.5	0.76	18.8	0.7	22.9	1.0	475.2	66.6	18.81	0.66	NA	x
Fringe Spot 27	855	701677	0.4	11.3631	1.1	2.7590	3.3	0.2275	3.1	0.94	1321.3	37.0	1344.5	24.6	1382.6	22.0	1382.55	22.01	95.6	x
Fringe Spot 29	486	339384	0.2	20.2390	1.2	0.1476	4.0	0.0217	3.8	0.95	138.2	5.2	139.7	5.2	167.3	28.7	138.19	5.19	NA	x
Fringe Spot 30	158	2759	1.2	22.1228	4.0	0.0184	5.5	0.0030	3.7	0.68	19.0	0.7	18.5	1.0	NA	NA	19.04	0.70	NA	
Fringe Spot 32	594	2191839	0.1	9.6260	1.2	4.1367	3.7	0.2889	3.5	0.95	1636.2	50.8	1661.6	30.3	1694.6	21.8	1694.64	21.81	96.6	x
Fringe Spot 34	181	2868	0.5	23.8702	7.1	0.0169	7.6	0.0029	2.7	0.35	18.9	0.5	17.0	1.3	NA	NA	18.88	0.50	NA	
Fringe Spot 35	289	58128	0.7	20.4306	1.5	0.1605	3.0	0.0238	2.6	0.87	151.6	3.8	151.2	4.2	145.2	34.7	151.60	3.84	NA	x
<b>0204M1 (McClanahan Spring pluton, 35.68453, -115.16762)</b>																				
0204M1 Spot 1	978	10069	0.6	10.0427	1.1	2.2394	4.6	0.1632	4.5	0.97	974.4	40.4	1193.5	32.3	1616.1	20.1	1616.14	20.13	60.3	
0204M1 Spot 2	1117	16613	0.4	10.1877	1.1	2.6427	3.4	0.1954	3.2	0.95	1150.3	34.0	1312.6	25.1	1589.4	20.5	1589.41	20.48	72.4	
0204M1 Spot 3	946	11490	0.3	10.1096	1.1	2.0594	5.0	0.1511	4.9	0.98	906.9	41.4	1135.4	34.3	1603.8	20.1	1603.77	20.11	56.6	
0204M1 Spot 4	685	33034	0.4	10.1193	0.9	3.4314	5.4	0.2519	5.4	0.99	1448.5	69.7	1511.6	42.8	1602.0	16.2	1601.97	16.24	90.4	
0204M1 Spot 5	1278	44083	0.5	10.7658	1.0	2.2435	3.4	0.1752	3.3	0.96	1041.0	31.3	1194.7	23.9	1485.6	18.9	1485.55	18.85	70.1	
0204M1 Spot 6	1612	2532	0.7	9.5747	0.9	1.8825	4.8	0.1308	4.7	0.98	792.3	35.0	1074.9	31.7	1704.5	16.0	1704.49	16.02	46.5	
0204M1 Spot 7	1247	10126	0.7	10.1291	1.2	2.3825	4.8	0.1751	4.7	0.97	1040.2	44.8	1237.4	34.4	1600.2	21.5	1600.17	21.54	65.0	
0204M1 Spot 8	859	11481	0.2	10.3954	0.7	2.1738	4.3	0.1640	4.2	0.99	978.8	38.5	1172.7	29.9	1551.6	13.6	1551.60	13.61	63.1	
0204M1 Spot 9	1653	6677	0.5	10.2358	1.7	2.2248	7.9	0.1652	7.8	0.98	985.8	70.9	1188.9	55.7	1580.6	31.5	1580.59	31.54	62.4	
0204M1 Spot 10	1406	3850	0.6	9.7207	0.7	1.7249	5.6	0.1217	5.6	0.99	740.1	39.2	1017.8	36.3	1676.6	12.1	1676.58	12.14	44.1	
0204M1 Spot 11	1091	6172	0.2	10.0576	0.8	2.5887	4.8	0.1889	4.8	0.99	1115.5	48.7	1297.5	35.3	1613.4	14.3	1613.37	14.26	69.1	
0204M1 Spot 12	808	105158	0.0	10.1100	0.9	3.9341	2.5	0.2886	2.4	0.94	1634.5	34.5	1620.7	20.6	1603.7	16.3	1603.70	16.29	101.9	
0204M1 Spot 13	1078	29557	0.3	10.6848	1.3	2.6740	3.6	0.2073	3.4	0.93	1214.5	37.5	1321.3	26.9	1499.8	24.9	1499.85	24.88	81.0	
0204M1 Spot 14	814	18685	0.1	10.0870	1.1	3.4097	3.2	0.2496	3.1	0.95	1436.2	39.6	1506.6	25.5	1607.9	19.6	1607.94	19.59	89.3	
0204M1 Spot 15	468	24782	0.0	9.8694	0.7	4.0474	2.4	0.2898	2.2	0.95	1640.7	32.5	1643.8	19.2	1648.5	13.5	1648.49	13.47	99.5	
0204M1 Spot 16	1038	16579	0.5	10.3289	1.0	2.3788	4.5	0.1783	4.3	0.97	1057.6	42.4	1236.2	31.9	1563.6	18.8	1563.64	18.80	67.6	
0204M1 Spot 17	1287	2322	0.5	9.2221	0.8	1.7067	6.0	0.1142	5.9	0.99	697.1	39.0	1011.1	38.2	1773.3	14.6	1773.27	14.56	39.3	
0204M1 Spot 18	124	10454	0.4	9.4679	1.0	4.1790	2.8	0.2871	2.6	0.93	1627.0	37.4	1669.9	22.9	1725.1	18.6	1725.13	18.57	94.3	
0204M1 Spot 20	1659	20446	0.5	11.4207	1.2	1.7143	3.2	0.1421	3.0	0.93	856.3	24.1	1013.9	20.8	1372.8	23.2	1372.84	23.16	62.4	
0204M1 Spot 21	1703	5749	0.7	10.6418	1.2	1.5868	6.8	0.1225	6.7	0.98	745.1	46.9	965.0	42.2	1507.5	23.1	1507.48	23.07	49.4	
0204M1 Spot 22	1046	15233	0.2	10.3511	0.8	2.2847	3.5	0.1716	3.4	0.97	1020.9	31.8	1207.6	24.5	1559.6	15.4	1559.60	15.43	65.5	
0204M1 Spot 23	1591	14765	0.4	10.7196	0.8	2.5754	5.6	0.2003	5.5	0.99	1177.0	59.4	1293.7	40.9	1493.7	16.1	1493.71	16.08	78.8	
0204M1 Spot 24	1145	7674	0.4	10.5694	0.7	1.9885	4.7	0.1525	4.6	0.99	915.0	39.2	1111.6	31.5	1520.4	14.0	1520.36	13.98	60.2	
0204M1 Spot 25	249	66668	0.2	9.5670	0.8	4.2087	3.1	0.2921	3.0	0.97	1652.3	43.7	1675.7	25.4	1706.0	14.5	1705.98	14.48	96.9	
0204M1 Spot 26	1572	7850	0.5	10.8441	0.8	4.4708	5.4	0.1157	5.3	0.99	705.9	35.7	918.5	32.7	1471.8	16.0	1471.83	16.03	48.0	
0204M1 Spot 27	1644	3238	1.0	9.9562	1.3	2.0872	7.9	0.1508	7.8	0.99	905.3	65.9	1144.6	54.4	1632.2	24.9	1632.22	24.94	55.5	
0204M1 Spot 28	1309	17328	0.6	11.0994	1.0	1.9254	5.6	0.1551	5.5	0.98	929.3	47.6	1090.0	37.4	1427.5	18.8	1427.52	18.83	65.1	
0204M1 Spot 29	1576	8479	0.6	10.2967	0.9	2.3895	6.4	0.1785	6.4	0.99	1058.9	62.1	1239.5	46.0	1569.5	16.3	1569.49	16.31	67.5	
0204M1 Spot 30	954	9578	0.7	9.6945	1.0	1.9809	5.6	0.1393	5.6	0.98	840.9	43.8	1109.0	38.1	1681.6	18.0	1681.57	18.02	50.0	
0204M1 Spot 31	1453	14859	0.4	10.5992	1.3	2.5464	6.3	0.1958	6.2	0.98	1152.9	65.3	1285.4	46.1	1515.1	23.9	1515.05	23.93	76.1	
0204M1 Spot 32	639	36922	0.5	10.0509	1.0	2.6873	3.1	0.1960	2.9	0.94	1153.7	30.9	1325.0	23.0	1614.6	19.3	1614.63	19.27	71.5	
0204M1 Spot 33	1131	18482	0.6	10.3342	1.0	2.3014	3.0	0.1726	2.8	0.95	1026.3	26.7	1212.7	21.0	1562.7	18.0	1562.67	17.97	65.7	
0204M1 Spot 34	801	31103	0.4	10.2734	0.9	3.2431	3.5	0.2417	3.4	0.97	1395.8	42.2	1467.5	27.0	1573.7	16.5	1573.73	16.50	88.7	
0204M1 Spot 35	1372	15542	0.4	10.6161	0.9	1.9268	4.1	0.1484	3.9	0.97	892.1	32.9	1090.4	27.1	1512.0	17.8	1512.04	17.83	59.0	
<b>BBP4 (Xbbp, 35.73587, -115.18277)</b>																				
BBP4 Spot 2	187	274338	0.8	9.8195	1.0	4.0871	3.0	0.2912	2.9	0.94	1647.5	41.8	1651.7	24.9	1657.9	18.6	1657.9	18.6	99.4	

Analysis	U	206Pb	Th/U	206Pb*	±	207Pb*	±	206Pb*	±	error	206Pb*	±	207Pb*	±	206Pb*	±	Best age	±	Conc	Ex *
BBP4 Spot 3	260	130869	0.4	9.7995	1.1	4.0111	3.8	0.2852	3.6	0.96	1617.5	52.1	1636.4	30.9	1661.6	20.0	1661.6	20.0	97.3	
BBP4 Spot 4	119	1052971	0.3	9.7548	1.0	4.0411	2.7	0.2860	2.5	0.93	1621.6	35.7	1642.5	21.7	1670.1	17.9	1670.1	17.9	97.1	
BBP4 Spot 5	376	4291547	0.2	9.6325	1.0	4.1495	3.1	0.2900	2.9	0.95	1641.6	42.0	1664.1	25.0	1693.4	17.9	1693.4	17.9	96.9	
BBP4 Spot 6	333	81859	0.4	9.8842	1.0	4.1265	2.7	0.2959	2.5	0.93	1671.2	36.8	1659.6	22.0	1645.7	18.5	1645.7	18.5	101.5	
BBP4 Spot 7	889	230862	0.3	10.1684	1.2	3.9072	3.1	0.2883	2.8	0.93	1632.9	41.0	1615.2	24.8	1592.9	21.8	1592.9	21.8	102.5	
BBP4 Spot 8	196	302280	0.6	9.8055	1.0	4.1110	2.4	0.2925	2.2	0.91	1653.9	31.9	1656.5	19.7	1660.5	18.7	1660.5	18.7	99.6	
BBP4 Spot 9	79	24557	0.6	9.6077	0.9	3.9558	2.8	0.2758	2.6	0.95	1570.0	36.7	1625.2	22.5	1698.2	16.1	1698.2	16.1	92.5	x
BBP4 Spot 10	842	1731015	0.3	10.0324	0.8	4.0868	2.9	0.2975	2.8	0.96	1678.9	41.3	1651.7	23.8	1618.1	15.8	1618.1	15.8	103.8	
BBP4 Spot 11	645	719099	0.2	9.7625	1.0	3.6048	2.6	0.2553	2.4	0.93	1466.0	32.0	1550.6	20.9	1668.7	18.0	1668.7	18.0	87.9	x
BBP4 Spot 12	143	115092	0.4	9.7848	0.8	4.2037	2.5	0.2985	2.3	0.94	1683.6	34.3	1674.7	20.1	1664.4	15.2	1664.4	15.2	101.2	
BBP4 Spot 14	159	2032016	0.4	9.7958	0.8	4.1968	2.8	0.2983	2.6	0.95	1682.8	39.0	1673.4	22.6	1662.3	15.3	1662.3	15.3	101.2	
BBP4 Spot 15	181	113944	0.4	9.7786	0.7	4.2201	2.4	0.2994	2.4	0.96	1688.5	35.0	1677.9	20.1	1665.6	12.1	1665.6	12.1	101.4	
BBP4 Spot 16	168	111958	0.4	9.8387	1.1	4.1965	2.9	0.2996	2.7	0.92	1689.2	40.1	1673.3	24.0	1654.3	20.9	1654.3	20.9	102.1	
BBP4 Spot 17	161	127170	0.4	9.7256	1.0	4.2052	2.9	0.2968	2.7	0.94	1675.2	39.7	1675.0	23.5	1675.6	18.3	1675.6	18.3	100.0	
BBP4 Spot 18	155	148580	0.3	9.8229	0.8	4.1880	2.5	0.2985	2.4	0.95	1683.8	35.2	1671.7	20.5	1657.2	14.4	1657.2	14.4	101.6	
BBP4 Spot 19	291	63043	0.4	9.8458	0.7	4.1365	3.0	0.2955	2.9	0.97	1669.0	43.4	1661.5	24.9	1652.9	13.7	1652.9	13.7	101.0	
BBP4 Spot 20	153	46952	0.4	9.9786	0.8	4.0752	2.9	0.2951	2.7	0.96	1666.8	40.4	1649.4	23.4	1628.0	15.5	1628.0	15.5	102.4	
BBP4 Spot 21	396	66373	0.5	9.5880	0.9	3.9279	2.9	0.2733	2.8	0.95	1557.3	38.5	1619.4	23.7	1701.9	16.7	1701.9	16.7	91.5	x
BBP4 Spot 23	574	1165939	0.3	9.8163	0.9	4.1422	2.4	0.2950	2.2	0.93	1666.6	32.2	1662.7	19.2	1658.5	15.8	1658.5	15.8	100.5	
BBP4 Spot 26	667	160309	0.2	10.0017	0.9	4.0451	2.3	0.2936	2.1	0.92	1659.3	30.4	1643.3	18.3	1623.7	16.2	1623.7	16.2	102.2	
BBP4 Spot 27	144	285967	0.4	9.7838	1.2	4.1458	3.0	0.2943	2.7	0.91	1663.0	39.6	1663.4	24.2	1664.6	22.1	1664.6	22.1	99.9	
BBP4 Spot 28	58	124217	0.5	9.8181	1.0	4.1323	2.6	0.2944	2.4	0.92	1663.4	35.3	1660.7	21.4	1658.1	19.3	1658.1	19.3	100.3	
BBP4 Spot 29	161	281204	0.5	9.6732	0.9	4.2520	3.1	0.2984	3.0	0.96	1683.6	44.4	1684.1	25.7	1685.6	16.9	1685.6	16.9	99.9	
BBP4 Spot 30	196	293580	0.4	9.8332	0.8	4.0713	2.5	0.2905	2.3	0.95	1643.9	33.8	1648.6	20.0	1655.3	14.3	1655.3	14.3	99.3	
BBP4 Spot 32	469	113045	0.5	9.7353	1.1	4.1171	2.7	0.2908	2.4	0.92	1645.7	35.5	1657.7	21.8	1673.8	19.5	1673.8	19.5	98.3	
BBP4 Spot 33	643	288092	0.3	9.9386	1.3	4.1398	3.1	0.2985	2.8	0.91	1684.0	41.1	1662.2	24.9	1635.5	23.6	1635.5	23.6	103.0	
BBP4 Spot 34	142	120409	0.4	9.8160	1.1	4.1722	3.3	0.2972	3.1	0.95	1677.2	46.2	1668.6	27.1	1658.5	19.5	1658.5	19.5	101.1	
BBP4 Spot 34	126	45633	0.4	9.7952	1.0	4.0784	3.0	0.2899	2.8	0.94	1640.8	40.9	1650.0	24.5	1662.5	18.5	1662.5	18.5	98.7	
BBP4 Spot 35	94	58538	0.5	9.7593	1.1	4.1124	2.9	0.2912	2.7	0.93	1647.6	39.8	1656.8	23.9	1669.2	19.4	1669.2	19.4	98.7	
<b>BBP1 (Xbbp, 35.62819, -115.27303)</b>																				
BBP1 Spot 36	411	17424	0.6	9.4559	0.9	4.0638	2.9	0.2788	2.7	0.94	1585.4	37.9	1647.1	23.3	1727.5	17.2	1727.45	17.21	91.8	x
BBP1 Spot 37	367	37930	0.3	9.6128	1.2	4.1436	3.1	0.2890	2.9	0.93	1636.6	41.6	1662.9	25.4	1697.2	21.3	1697.18	21.35	96.4	
BBP1 Spot 38	138	38752	1.1	9.7990	1.0	4.2003	3.0	0.2986	2.8	0.95	1684.6	41.6	1674.1	24.3	1661.8	17.8	1661.75	17.83	101.4	
BBP1 Spot 39	227	49342	0.8	9.9039	0.9	4.1751	2.9	0.3000	2.8	0.96	1691.4	41.4	1669.1	23.8	1642.0	15.9	1642.01	15.92	103.0	
BBP1 Spot 40	134	7309	0.6	9.9783	1.2	4.0178	3.0	0.2909	2.7	0.92	1646.0	39.8	1637.8	24.2	1628.1	21.6	1628.10	21.62	101.1	
BBP1 Spot 41	238	48786	0.7	9.7200	1.1	3.7558	3.1	0.2649	3.0	0.94	1514.8	40.0	1583.3	25.2	1676.7	19.6	1676.72	19.63	90.3	x
BBP1 Spot 42	505	382040	0.4	9.8563	1.0	4.1282	2.6	0.2952	2.4	0.93	1667.6	35.1	1659.9	21.1	1650.9	18.1	1650.95	18.10	101.0	
BBP1 Spot 43	116	37366	0.5	9.8418	1.2	4.2171	2.7	0.3011	2.5	0.90	1697.0	37.0	1677.4	22.5	1653.7	21.8	1653.67	21.76	102.6	
BBP1 Spot 44	94	15801	0.5	9.8564	1.0	4.0781	3.1	0.2917	3.0	0.94	1649.8	43.1	1649.9	25.6	1650.9	19.0	1650.93	19.04	99.9	
BBP1 Spot 45	149	26485	0.6	9.8027	1.2	4.1797	3.2	0.2973	2.9	0.92	1677.9	43.3	1670.1	26.0	1661.0	22.8	1661.05	22.82	101.0	
BBP1 Spot 46	187	46330	0.6	9.7198	0.9	4.0970	2.7	0.2889	2.6	0.94	1636.2	36.9	1653.7	22.1	1676.8	16.9	1676.76	16.89	97.6	
BBP1 Spot 47	55	16523	0.7	9.7610	1.0	4.1725	2.6	0.2955	2.4	0.92	1669.0	35.3	1668.6	21.4	1668.9	19.4	1668.92	19.40	100.0	
BBP1 Spot 48	173	153670	0.6	9.6877	0.9	4.2199	2.8	0.2966	2.7	0.95	1674.6	39.7	1677.9	23.4	1682.9	17.0	1682.85	17.04	99.5	
BBP1 Spot 49	327	145398	0.3	9.6985	0.8	3.9579	2.3	0.2785	2.2	0.94	1583.9	30.9	1625.6	18.9	1680.8	14.5	1680.81	14.55	94.2	
BBP1 Spot 50	227	88295	0.7	9.7006	0.9	4.0455	3.3	0.2847	3.1	0.96	1615.2	44.9	1643.4	26.6	1680.4	16.3	1680.40	16.26	96.1	
BBP1 Spot 51	94	18488	0.7	9.9433	1.2	4.0898	2.8	0.2951	2.5	0.91	1666.8	36.8	1652.3	22.6	1634.6	21.7	1634.64	21.66	102.0	
BBP1 Spot 52	310	68325	0.5	9.7270	0.9	4.0538	2.7	0.2861	2.5	0.94	1622.1	36.0	1645.1	21.8	1675.4	17.0	1675.38	16.98	96.8	
BBP1 Spot 53	195	196614	0.5	9.6925	0.9	4.2251	2.9	0.2971	2.8	0.95	1677.1	41.4	1678.9	24.2	1681.9	16.6	1681.94	16.62	99.7	
BBP1 Spot 54	350	446009	0.5	9.5962	1.1	4.2050	2.3	0.2928	2.0	0.88	1655.5	29.7	1675.0	19.0	1700.4	20.2	1700.36	20.22	97.4	
BBP1 Spot 55	358	82484	0.4	9.3579	1.1	4.5171	2.4	0.3067	2.2	0.90	1724.5	33.2	1734.1	20.3	1746.5	19.5	1746.54	19.49	98.7	
BBP1 Spot 56	133	25780	0.6	9.7753	1.1	4.1261	3.1	0.2927	2.9	0.94	1654.8	42.1	1659.5	25.1	1666.2	19.6	1666.23	19.64	99.3	

Analysis	U	206Pb	Th/U	206Pb*	±	207Pb*	±	206Pb*	±	error	206Pb*	±	207Pb*	±	206Pb*	±	Best age	±	Conc	Ex *
BBP1 Spot 57	70	42460	1.0	9.9070	0.8	4.1534	2.6	0.2986	2.4	0.95	1684.2	36.0	1664.9	21.0	1641.4	15.5	1641.43	15.48	102.6	
BBP1 Spot 58	384	140040	0.6	9.7390	0.9	4.0366	3.0	0.2852	2.8	0.95	1617.7	40.6	1641.6	24.3	1673.1	17.2	1673.11	17.19	96.7	
BBP1 Spot 59	360	52454	0.6	9.8768	0.7	4.1299	2.7	0.2960	2.6	0.96	1671.3	38.0	1660.2	22.0	1647.1	13.8	1647.09	13.82	101.5	
BBP1 Spot 60	283	102350	0.4	9.7959	1.0	4.1737	2.8	0.2967	2.6	0.93	1674.7	38.2	1668.9	22.7	1662.3	18.3	1662.32	18.26	100.7	
BBP1 Spot 61	331	247438	0.6	9.6448	1.1	4.1342	2.7	0.2893	2.4	0.90	1638.1	35.1	1661.1	21.9	1691.1	21.1	1691.05	21.13	96.9	
BBP1 Spot 62	183	77481	0.6	9.8303	1.1	4.1554	3.1	0.2964	2.9	0.94	1673.4	43.0	1665.3	25.4	1655.8	19.6	1655.83	19.57	101.1	
BBP1 Spot 63	74	12929	0.5	9.9900	1.1	3.9566	2.9	0.2868	2.7	0.93	1625.5	38.5	1625.3	23.4	1625.9	20.2	1625.93	20.23	100.0	
BBP1 Spot 64	227	19414	0.3	9.4973	0.9	4.0476	3.0	0.2789	2.9	0.95	1585.9	40.5	1643.8	24.7	1719.4	17.4	1719.42	17.40	92.2	x
BBP1 Spot 65	250	80491	0.6	9.6800	1.0	4.1474	3.3	0.2913	3.1	0.95	1648.0	45.7	1663.7	27.1	1684.3	19.3	1684.33	19.27	97.8	
BBP1 Spot 66	56	26637	0.7	9.5457	1.2	4.2625	2.5	0.2952	2.2	0.88	1667.6	32.2	1686.2	20.5	1710.1	21.9	1710.07	21.95	97.5	
BBP1 Spot 67	658	143389	0.4	9.8491	1.2	3.8305	3.3	0.2737	3.0	0.93	1559.8	42.0	1599.2	26.3	1652.3	22.7	1652.29	22.74	94.4	
BBP1 Spot 68	156	39806	0.5	9.7712	1.1	4.0883	3.1	0.2898	2.9	0.94	1640.8	42.2	1652.0	25.3	1667.0	19.5	1667.01	19.47	98.4	
BBP1 Spot 69	122	24818	0.5	9.7760	1.0	4.2160	3.2	0.2991	3.0	0.94	1686.6	44.3	1677.1	25.9	1666.1	19.2	1666.09	19.21	101.2	
BBP1 Spot 70	267	79426	0.5	9.6599	1.0	4.0775	2.9	0.2858	2.7	0.93	1620.5	39.1	1649.8	23.9	1688.2	19.3	1688.17	19.29	96.0	

\*Ex—analysis excluded from determination of the mean age.

Laser ablation multicollector inductively coupled plasma mass spectrometry (LA-MC-ICPMS) analyses conducted at the Arizona LaserChron Center.

1. All uncertainties are reported at the 1-sigma level, and include only measurement errors.

2. Analyses conducted by LA-MC-ICPMS, as described by Gehrels et al. (2008).

3. U concentration and U/Th are calibrated relative to Sri Lanka zircon standard and are accurate to ~20%.

4. Common Pb correction is from measured  $^{204}\text{Pb}$  with common Pb composition interpreted from Stacey and Kramers (1975).

5. Common Pb composition assigned uncertainties of 1.5 for  $^{206}\text{Pb}/^{204}\text{Pb}$ , 0.3 for  $^{207}\text{Pb}/^{204}\text{Pb}$ , and 2.0 for  $^{208}\text{Pb}/^{204}\text{Pb}$ .

6. U/Pb and  $^{206}\text{Pb}/^{207}\text{Pb}$  fractionation is calibrated relative to fragments of a large Sri Lanka zircon of  $563.5 \pm 3.2$  Ma (2-sigma).

7. U decay constants and composition as follows:  $^{235}\text{U} = 9.8485 \times 10^{-10}$ ,  $^{238}\text{U} = 1.55125 \times 10^{-10}$ ,  $^{238}\text{U}/^{235}\text{U} = 137.88$ .